TEST WAVEFORMS FOR IMMUNITY OF AVIONIC SYSTEMS TO THE ELECTROMAGNETIC INTERFERENCE OF PORTABLE ELECTRONIC DEVICES

FORMES D'ONDES DE TEST POUR L'IMMUNITÉ DES SYSTÈMES AVIONIQUES AUX PERTURBATIONS ÉLECTROMAGNÉTIQUES DES APPAREILS ELECTRONIQUES PORTATIFS

A Thesis Submitted to the Division of Graduate Studies
of the Royal Military College of Canada
by

Samuel Blanchette, BEng, rmc
Captain

In Partial Fulfillment of the Requirements for the Degree of
Master of Applied Science in Electrical Engineering

June, 2017

À Dulcie

Acknowledgements

I would like to thank my co-supervisors, Dr. Joey Bray and Dr. Yahia Antar, for their unfailing support for the duration of my studies at the Royal Military College of Canada. This thesis would not have been possible without their help and their guidance. I would also like to thank Mr. Serge Couture from the Aerospace Engineering Test Establishment (AETE), for sharing his comprehensive knowledge on the subjects of Electromagnetic Interference and Compatibility testing. I would finally like to thank the Director Technical Airworthiness & Engineering Support for their funding.

Abstract

Avionic systems are susceptible to electromagnetic interference (EMI) caused by portable electronic devices (PEDs). In order to allow the use of PEDs in the aircraft cockpit environment, radiated susceptibility testing must be performed. However, current test signals are not representative of modern telecommunication standards: characteristics of the communications signals, such as the frequency bandwidth and the peak to average power ratio (PAPR), are not emulated.

This work describes the analysis of complex telecommunication signals such as Long Term Evolution (LTE). Different waveforms are proposed to modulate the signals used in radiated susceptibility testing. Avionic equipment is tested in an anechoic chamber, and the EMI is measured. The measurements associated with the different test waveforms are compared to determine how the characteristics of the signals can affect the level of interference.

Résumé

Les systèmes avioniques sont susceptibles aux interférences électromagnétiques (EMI) causées par les appareils électroniques portatifs (AEP). Pour pouvoir autoriser l'usage des AEP dans le cockpit des aéronefs, des tests de susceptibilité aux rayonnements doivent être entrepris. Cependant, les signaux de tests actuels ne sont pas représentatifs des standards de télécommunications modernes : certaines caractéristiques des signaux de communications, telles que la largeur de bande et le rapport de la puissance de crête à la puissance moyenne, ne sont pas reproduites.

Ce travail fait une analyse de signaux de télécommunications complexes tels que Long Term Evolution (LTE). Différentes formes d'ondes sont proposées pour moduler les signaux utilisés dans les tests de susceptibilité aux rayonnements. De l'équipement avionique est testé en chambre anéchoïque, et les interférences électromagnétiques sont mesurées. Les mesures associées aux différentes formes d'onde de test seront comparées pour déterminer comment les caractéristiques du signal peuvent affecter le niveau d'interférence.

Contents

List of Tables

List of Figures

List of Acronyms

CCDF	Complementary Cumulative Distribution Function
CSV	Comma-Separated Values
DMRS	Demodulation Reference Signals
DoD	United States Department of Defense
DTx	Discontinuous Transmission
DUT	Device Under Test
EMC	Electromagnetic Compatibility
EMI	Electromagnetic Interference
FCC	Federal Communications Commission
FDD	Frequency Division Duplexing
FDMA	Frequency Division Multiple Access
GMSK	Gaussian Minimum Shift Keying
GSM	Global System for Mobile communications
HIRF	High Intensity Radiated Fields
IBS	Isotropic Broadband Susceptibility
IEC	International Electrotechnical Commission
LTE	Long Term Evolution
MCS	Modulation Coding Scheme
OBW	Occupied Bandwidth
OFDM	Orthogonal Frequency Division Multiplexing
PAPR	Peak to Average Power Ratio
PDF	Probability Density Function
PED	Portable Electronic Devices
PRACH	Physical Random Access Channel
PRF	Pulse Repetition Frequency
PSD	Power Spectral Density
PUCCH	Physical Uplink Control Channel

PUSCH	Physical Uplink Shared Channel
QAM	Quadrature Amplitude Modulation
QPSK	Quadrature Phase Shift Keying
RBW	Resolution Bandwidth
RRC	Root Raised Cosine
RTCA	Radio Technical Commission for Aeronautics
SC-FDMA	Single Carrier FDMA
SEM	Spectrum Emission Mask
SRS	Sounding Reference Signal
TDD	Time Division Duplexing
TDMA	Time Division Multiple Access
UMTS	Universal Mobile Telecommunications System
VSA	Vector Signal Analyzer
VSG	Vector Signal Generators
W-CDMA	Wideband Code Division Multiple Access

1 Introduction

1.1 Background

Portable Electronic Devices (PEDs) such as mobile phones and portable computers are replacing paper publications in the aircraft cabin. These devices, known as electronic flight bags, are routinely used by the crew. By their nature, PEDs transmit electromagnetic radiation in the form of intentional and non-intentional emissions. These emissions pose a risk Electromagnetic Interference (EMI): they can disturb the normal function of the avionic systems, which can lead to disastrous consequences if the affected systems are flight safety-critical.

Allowing the use of PEDs in the aircraft cockpit environment is an old issue: the Radio Technical Commission for Aeronautics (RTCA), a private not-for-profit organization, has been studying the problem for over 30 years. To simplify the EMI analysis, the interference coupling path between the source and the victim are categorized in two types: front-door coupling, and back-door coupling. Front-door coupling is the transmission of electromagnetic energy through an entry that was designed to receive a signal during normal operation; back-door coupling is the transmission of energy through an entry of which the function is not to receive a signal. In this thesis, only the back-door coupling interference will be studied.

To allow the use of PEDs in the aircraft cabin environment, aviation authorities must ensure the immunity of the avionic systems to the different types of EMI. Back-door immunity to intentional PED emissions can be verified by radiated susceptibility testing: a signal is transmitted in proximity to an avionic system, and the response of the system is monitored to detect any disturbance.

RTCA document 294C proposed a list of test waveforms to emulate the communications standards that were current when the document was published in 2008 [4]. Such waveforms were recommended for use in radiated susceptibility

testing, to ensure that the avionic systems were not affected by communication signals that could be emitted by the PEDs.

The most recent recommendations by the RTCA mark a departure from previous guidance. RTCA document 307A recommended the use of a continuous signal for radiated susceptibility testing; similar to the signal used for high intensity radiated fields (HIRF) testing [5]. It argued that existing HIRF protection could provide some immunity to PED emissions. It proposed that the waveforms from document 294C can be used for additional testing; however the test waveforms were not updated to include the most recent communication standards.

1.2 Problem Statement

The aeronautical industry is motivated in allowing the use of PEDs inside the aircraft cabin to replace paper publications. However, testing for EMI immunity to complex communication standards is challenging. With the advent of vector signal generators, there is an interest for the use of complex waveforms that are closer to the real interfering signal. Test waveforms must have enough simplicity to ensure their repeatability, and reduce the testing time to a minimum. Few publications are available on the subject of EMI susceptibility to intentional radiated emissions with back-door coupling. Finally, there is no consensus in the Electromagnetic Compatibility (EMC) industry standards or in published literature on the type of waveforms that can be used to simulate the interference effects of the Long Term Evolution (LTE) communication standard.

1.3 Thesis Statement

EMI immunity to complex communication standards such as LTE can be tested using waveforms with reduced parameters. The objective of this research is to develop waveforms that are representative of the LTE communication standard, with enough simplicity for practical use in radiated susceptibility testing.

1.4 Methodology

In order to design test waveforms that are representative of LTE, it is necessary that they share the same signal properties. The first step of this thesis is to study the LTE communication standard: the characteristics of LTE that are suspected to have an effect on the back-door interference will be described, and LTE signals will be analyzed. Second, the waveforms that will be used in radiated susceptibility testing will be developed: a parameters reduction process will used to obtain test waveforms with properties that are similar to LTE waveforms. Third, radiated susceptibility testing will determine if the test waveforms are valid waveforms for use in EMI testing of the LTE standard.

1.5 Thesis Outline

Chapter 2 will survey the current EMC standards to compare the recommended test waveforms, and review the state of research on radiated susceptibility testing. Chapter 3 will provide a summary of the LTE standard, with the properties that make it different from other communication standards. The occupied bandwidths and the peak to average power ratio will be measured in LTE signal recordings. Chapter 4 will explain the design of test waveforms. LTE, SC-FDMA, QPSK, noise, and pulse modulated signals will be developed in accordance with the spectrum emission mask of LTE, for five different channel bandwidths. Chapter 5 will cover the radiated susceptibility testing with the waveforms. An avionic system will be chosen to become the device under test. The RMS and the peak power of the interference induced by the different waveforms will be measured for multiple carrier frequencies. The radiated test results will be analyzed to determine the validity of the test waveforms. Chapter 6 will conclude this thesis, and will propose future research work on the subject of radiated susceptibility testing.

2 Literature survey

The most basic decomposition of any EMI problem has three elements: an emitter, a coupling path, and a receiver [1]. In the context of this research, the mobile device is the emission source, and any aircraft electronic system can become a receiver. The coupling path is the transfer of electromagnetic energy though the aircraft environment, as shown in Fig. 2.1. In this chapter, different aspects of the source, the coupling path, and the receiver will be studied.

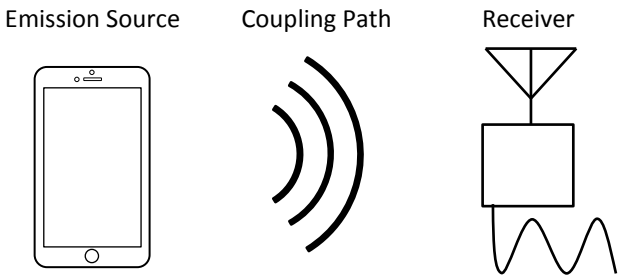

Figure 2.1: EMI threat model

2.1 Commercial Mobile Communication Emission sources

Personal electronic devices (PEDs) are required to adhere to standards for their emissions. In the USA, the Federal Communications Commission (FCC) regulates electromagnetic radiation from electronic devices, restricting the field strength of emissions radiated within specified frequency bands. In Canada, the Spectrum Management branch of Innovation, Science and Economic Development Canada (previously Industry Canada) specifies the emission limits in certification requirements for electronic devices. Although modern PEDs can use various wireless protocols, including Bluetooth and Wi-Fi, we will restrict our attention to two mobile telephony standards only, namely the Global System for Mobile communications (GSM) and Long Term Evolution (LTE).

2.1.1 The Global System for Mobile Communications (GSM)

The GSM communication standard is a second generation (2G) mobile telecommunications technology [2]. GSM uses time division multiple access (TDMA), in which time slots are allocated to different users on the same frequency channels. The GSM frame structure is composed of TDMA frames with a length of 4.6 ms. GSM uses a separation of 200 kHz between each frequency channel, with a frequency hopping sequence to reduce interference between adjacent channels. GSM uses Gaussian Minimum Shift Keying (GMSK) modulation: the data is modulated on the carrier signal by changing the phase of the carrier.

An important aspect of GSM is its discontinuous transmission (DTx). DTx is a state where bursts can only be transmitted during specific TDMA frames to reduce power consumption of the mobile device when continuous voice transmission is not required. DTx also helps to reduce interference between GSM devices.

2.1.2 Long Term Evolution (LTE)

The Long Term Evolution (LTE) communication standard is a fourth generation (4G) mobile telecommunications technology [3]. LTE uses TDMA, but also frequency division multiple access (FDMA): specific time slots and frequencies within a channel are allocated to different users.

LTE uses the single carrier FDMA (SC-FDMA) to transmit data in uplink channels. SC-FDMA is similar to the orthogonal frequency division multiplexing (OFDM) used in Wi-Fi, in that the channel bandwidth is mapped into subcarriers. Chapter 3 will discuss the important characteristics of the LTE communication standard in further detail.

2.2 Interference coupling paths

The EMC standard DO294C classifies two types of coupling path: front-door, and back-door [4]. Front-door coupling is the transmission of EM energy through an entry point whose function is to receive a signal during normal operation of the victim system [4]. Front door coupling occurs when a signal is coupled to the antenna connected to a receiver, as shown in Fig. 2.2. Many studies have been published on the effects of front door coupling in an aircraft cabin environment [5].

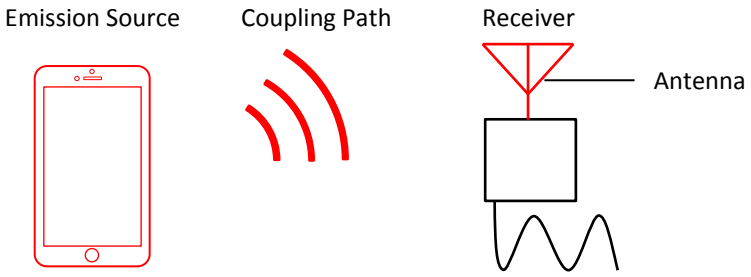

Figure 2.2: Front-door coupling to a victim system

Back-door coupling is the transmission of EM energy through an entry point of the victim system which function is not to receive a signal [4]. Back-door coupling occurs when the EM energy is directly coupled to the internal electronic components of a receiver, or coupled to its cables, as shown in Fig. 2.3. Few studies have been published on the effects of back-door coupling [8] [9].

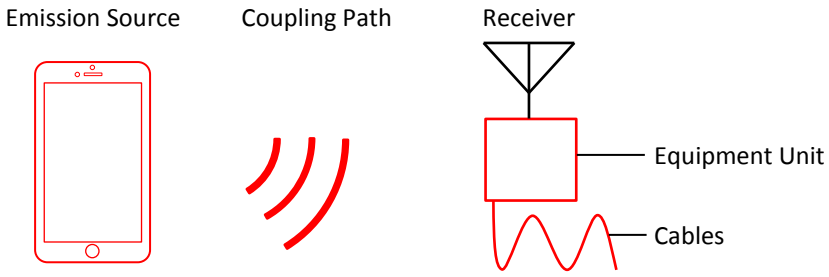

Figure 2.3: Back-door coupling to a victim system

2.3 EMC Standards

EMC standards provide guidance on the emission and susceptibility tests necessary to certify a product's conformance. Publications from three EMC standards organizations were reviewed for the purpose of this project: the Radio Technical Commission for Aeronautics (RTCA), the International Electrotechnical Commission (IEC), and the United States Department of Defense (DoD). Each of these organizations has a different vision in the development of EMC standards, and they recommend different waveforms for EMI susceptibility testing.

2.3.1 Radio Technical Commission for Aeronautics (RTCA)

The RTCA's role is to offer technical recommendations to civil aviation authorities and to the aerospace industry. DO294C provides a framework for the characterization of PEDs: it describes coupling paths in an aircraft configuration, and it sets EMI susceptibility levels for aircraft systems [4].

For the purpose of EMI susceptibility testing of aircraft systems, DO294C proposes a list of test waveforms corresponding to specific communication standards. Two types of waveforms are proposed: pulse modulated waveforms, and continuous waveforms. To emulate a communication standard using TDMA such as GSM, DO294C recommends a pulse modulated signal, with a pulse repetition frequency (PRF) of 217 Hz, and a duty cycle of 1:8, as shown in Fig. 2.4.

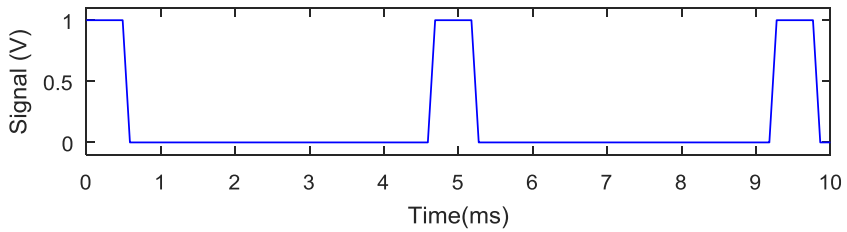

Figure 2.4: Pulse modulation with a PRF of 217 Hz and a duty factor of 1:8

DO294C claims that phase modulation such as GMSK can be modeled by a continuous wave, and that the effect of the peak signal power is more significant than the effect of the signal energy. DO294C recommends the derivation of extended waveforms for additional susceptibility testing. To emulate a PED using a communication standard with complex modulation such as OFDM used in Wi-Fi, DO294C recommends using a filtered white Gaussian noise, with a high peak to average power ratio (PAPR).

2.3.2 International Electrotechnical Commission (IEC)

The IEC publishes international standards for electrical, electronic and related technologies. IEC 61000-4-3 is a standard for radiated immunity testing and measurements techniques [6]. It proposes three modulation methods for radiated susceptibility testing. The first method is a sine wave amplitude modulation with a frequency of 1 kHz and a modulation depth of 80%. The second method is a square wave modulation with a PRF of 200 Hz, and a duty cycle of 1:2. The third method is a pulse modulation with a duty cycle and a PRF that correspond to a specific communication standard. For GSM, 61000-4-3 recommends a pulse modulation with a PRF of 217 Hz and, a duty cycle of 1:8, similar to DO294C.

In addition, IEC 61000-4-3 introduces a secondary modulation parameter: a pulse repetition frequency (PRF) of 2 Hz that can be used to simulate the discontinuous transmission (DTx) in GSM. Secondary modulation of a pulse waveform results in a burst of pulses, as shown in Fig. 2.5.

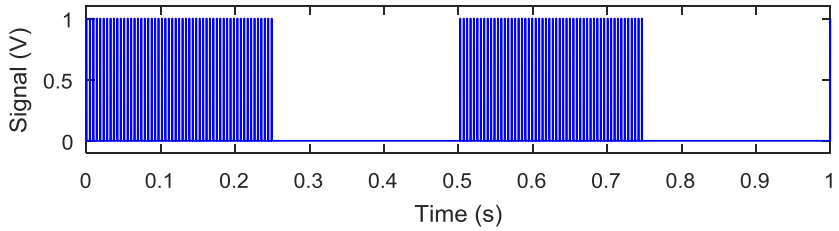

Figure 2.5: Burst of pulses resulting from secondary modulation

2.3.3 United States Department of Defense (DoD)

MIL-STD-461 is a standard published by the DoD to establish EMI emission and susceptibility requirements for equipment designed or purchased by the DoD [7]. The requirements for radiated susceptibility to the electric field are outlined in section RS103 of MIL-STD-461: aircraft safety critical equipment must be tested to electric field strengths of 200 V/m for frequencies from 2 MHz to 40 GHz. Other aircraft equipment must be tested to 20 V/m from 2 MHz to 1 GHz, and to electric field strengths of 60 V/m for frequencies from 1 GHz to 40 GHz.

MIL-STD-461 indicates that the susceptibility test signals shall be a pulse modulated signal with a PRF of 1 kHz and a duty cycle of 50%. The reason for the choice of a PRF 1 kHz is because it normally falls within the range of frequencies that can pass through audio and video filters of certain subsystems with a low frequency response characteristic, such as aircraft flight control subsystems.

2.3.4 Comparison of radiated susceptibility waveforms

All three EMC standard organizations recommended the use of a pulse modulated waveform to test for the radiated susceptibility of communications standards with TDMA. RTCA DO294C and IEC 61000-4-3 provided the same waveform parameters to emulate the GSM: a PRF of 217 Hz and a duty cycle of 1:8. The pulse modulated waveform can easily be reproduced in a testing environment. However, no recommendations were given on the pulse's rise time when testing for radiated susceptibility. A faster rise time could increase the frequency content of the pulse modulated waveform, and could have an effect on the victim systems.

None of the EMC standards provided a test waveform for the LTE communication standard. DO294C recommends the use of filtered white Gaussian noise to emulate OFDM signals; neither the IEC 61000-4-3 nor the MIL-STD-461 proposed additional waveforms to emulate complex communication standards. The existing waveforms are simple, but not representative of the signals used in LTE.

2.4 Radiated susceptibility studies

Several radiated susceptibility studies were reviewed for the purpose of this thesis. However, few studies were relevant to the derivation of waveforms for radiated susceptibility testing in an aircraft cockpit environment. In this section, four research publications on the study of test waveforms for radiated susceptibility will be presented. These studies provided a starting point for the design of test waveforms to be used in the context of radiated susceptibility to the LTE standard.

2.4.1 Isotropic Broadband Susceptibility (IBS) method

A study performed at the Naval Air Warfare Center compared the Isotropic Broadband Susceptibility (IBS) method to the RS103 method for EMI testing with back-door coupling [8]. The IBS method uses a band limited white Gaussian noise, such as described in DO294C. White Gaussian noise has the particularity of spreading the power over a large frequency band, and filtering the white Gaussian noise limits the frequency bandwidth of the signal. The IBS method was performed in a mode-stirred reverberating chamber: it has the advantage of illuminating the victim from all directions.

The RS103 method uses a pulse modulated signal, as described in section 2.4.3 [7]. It has a significantly lower frequency than the band limited white Gaussian noise. The RS103 method is typically performed in an anechoic chamber: multiple changes of antenna positions are required to illuminate the equipment under test.

The ARC-182 VHF/UHF Radio Receiver was chosen as a victim system for its narrow failure bandwidth, and the receiver was tested with both methods [8]. The IBS method was tested with noise bandwidths of 1.6, 6, 12, 22, and 56 MHz. The test was repeated with different carrier frequencies. Susceptibility thresholds were measured as the lowest electric field strength that caused a failure of the receiver. The IBS method discovered a susceptibility at 663 MHz that was not found during

the RS103 test. The susceptibility thresholds of the IBS method were higher than the susceptibility thresholds of RS103: higher field strengths were required for the IBS method than for RS103 to induce the same level of interference.

The author concluded that the IBS method could be used to replace RS103, because the susceptibilities found with RS103 were also found with the IBS method. The IBS method is also faster than for the RS103 method: fewer carrier frequency increments are required to cover the test frequencies, and fewer changes in the antenna positions are required to illuminate the equipment under test.

The main disadvantage of the IBS method is that the signal is difficult to reproduce with accuracy: the signals' frequency bandwidth was the only known characteristic of the noise generator. More research is required to establish the susceptibility thresholds associated with the IBS method. Vector signal generators could be used to transmit a signal that can be reproduced with higher accuracy.

2.4.2 Effect of modulated signal rise time

As discussed in section 2.3.4, the EMC standards did not provide recommendations on the modulated signal's rise time when testing for radiated susceptibility. To address this deficiency, a study performed at the NASA Langley Research Center evaluated the effects of the rise time [9]. The susceptibility thresholds relative were measured for three modulated signals: a square wave with a rise time of 630 ns, a square wave with a rise time of 14 ns, and a 1 μs pulse modulated signal with a rise time of 14 ns.

The signal with a rise time of 630 ns had higher susceptibility thresholds than both signals with a rise time of 14 ns: higher field strengths were required to induce the same level of interference. The authors concluded that the modulation rise time had a significant effect on EMI susceptibility. However, in order to design pulse waveforms for radiated susceptibility, it would be necessary to determine the rise times that are representative of specific communication standards.

2.4.3 Effect of the Peak to Average Power Ratio (PAPR)

A study performed at NTT DoCoMo research laboratories, Japan, evaluated the effect of the peak to average power ratio (PAPR) on medical devices [10]. PAPR, also known as crest factor or peak-to-average ratio, is a measure of the relative peak power of a signal, as expressed in (1.1)

$$PAPR[dB] = P_{Peak}[dB] - P_t[dB] \tag{1.1}$$

where P_{Peak} is the peak power, and P_t is the average power, expressed in decibels. A representation of signal waveforms with a high and low PAPR is shown in Fig. 2.6. Multicarrier modulation, such as SC-FDMA used in LTE standard, yields a higher PAPR than phase modulation, such as GMSK used in the GSM standard.

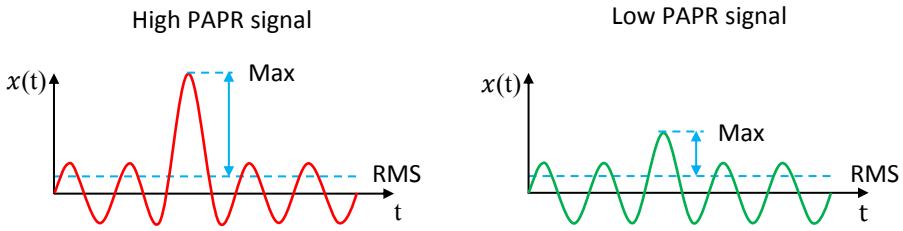

Figure 2.6: Signal waveforms with high and low PAPR

The authors compared the EMI effects of LTE and Wideband Code Division Multiple Access (W-CDMA) signals [10]. W-CDMA is a third generation (3G) mobile telecommunication technology, based on CDMA, a channel access method where specific codes are allocated to different users. CDMA is a spread spectrum technology, for the signal is spread on a large frequency bandwidth.

Two different releases of W-CDMA were used in this study: release 99, also known as the Universal Mobile Telecommunications System (UMTS), and release 6, also known as High Speed Packet Access (HSPA). W-CDMA release 99 and release 6 signals had PAPR values of 3.6 dB and 5.1 dB, respectively.

LTE release 8 signals were used, which had a PAPR of 7.7 dB. The PAPR values were for a complementary cumulative distribution function (CCDF) probability of 0.0001%: the PAPR was computed using one million samples.

The authors measured the maximum distance at which an EMI effect was observed [10]. The measurements were repeated for the three test signals using two transmitted power levels: a typical transmission power (10 dBm), and the maximum transmission power (23 or 24 dBm). Two carrier frequency bands were chosen to take the measurements: 2 GHz, and 800 MHz.

The authors found that the change in PAPR had no significant effect to the EMI disappearing distance, except for one case: using peak transmission power at 800 MHz, the W-CDMA release 6 signals had a slightly larger disappearing distance than the release 99 signals. All other signals had approximately the same EMI disappearing distance, independently of the peak transmission power.

These findings disagree with DO294C's suggestion that the peak signal power has a significant effect on the susceptibility. In order to determine the effect of PAPR, it would be necessary to perform additional radiation susceptibility testing with different PAPR values, while controlling the other parameters.

2.4.4 Effect of the discontinuous transmission mode

Another study performed at NTT Network Technology laboratories evaluated the effects of the discontinuous transmission mode on the interference to 32 different medical devices [11]. Similar to the previous study, the authors measured the EMI disappearing distance of three communication standards: the LTE, HSPA, and the Wideband Code Division Multiple Access (W-CDMA).

Two different transmission modes were chosen for susceptibility testing: a discontinuous mode, and a continuous mode. The discontinuous transmission mode had a pulse repetition interval of 1 s and a duty cycle of 50%. The pulse repetition interval was chosen to increase the susceptibility of medical devices used to detect

biological rhythms such as breathing and the heartbeat. The authors expected that discontinuous transmission mode would lead to induce higher levels of EMI [11].

Discontinuous waveforms were used to perform radiated susceptibility testing on all medical devices: 12 of the 32 medical devices were affected by the discontinuous transmissions. Then, the continuous waveforms were used to test only the medical devices for which EMI occurred in the discontinuous tests: 7 of the 12 medical devices tested were also affected by the continuous transmission. The maximum EMI disappearing distance was 80 cm for the discontinuous transmission, compared to 28 cm for the continuous transmission. The authors concluded that the discontinuous transmission mode could induce higher levels of interference to medical devices than the continuous transmission mode.

The authors did not use any of the test waveforms that are recommended by the EMC standards as a point of comparison to evaluate the radiated susceptibility of the medical devices. It is suspected that the discontinuous transmission mode can be emulated with a pulse modulated waveform; however this hypothesis cannot be validated without actual susceptibility measurement. Moreover, the authors gave no indication on the transition time between the transmitters on and off states.

2.4.5 Effect of the Orthogonal Frequency Division Multiplexing

A study performed at NTT Network Technology laboratories, Japan, evaluated the effect of the Orthogonal Frequency Division Multiplexing (OFDM) modulation for back-door radiated immunity tests in close proximity to equipment [12]. The effect of OFDM modulation was compared to pulse modulation (217 Hz, 50% duty cycle) and amplitude modulation (1 kHz, 80% depth). The OFDM signal had a discontinuous temporal waveform to emulate the IEEE 802.11 communication standard (Wi-Fi). The authors used two different test setups to perform the radiated immunity measurements. The first setup used a gigahertz transverse electromagnetic cell to expose the device under test (DUT) to an electric field with

gradually increasing field strength. The immunity levels were defined as the lowest field strengths which caused errors. The immunity levels were measured for the OFDM, pulse, and amplitude modulated signals. The immunity levels of the OFDM signal were found to be closer to the levels of the pulse modulated signal than the levels of the amplitude modulated signals.

The second setup used a double-ridged horn antenna. The antenna was positioned at a distance of 100 mm from the EUT. Because the size of the uniform electric field plane (20 cm x 8 cm) was smaller than the dimensions of the DUT, the surface of the DUT was divided into four areas. Measurements were taken with the antenna aligned on the center of each area. OFDM, pulse, and amplitude modulated signals were used to illuminate the DUT. In the first area, the immunity levels of the OFDM signal were significantly lower than the immunity levels of the pulse and amplitude modulated signals. In the three other areas, the immunity levels of the amplitude modulated signal were found to be almost always lower than the immunity levels of the OFDM signal and the pulse modulated signal. The authors concluded that the test method for radiated immunity testing should consider using a wideband signal such as an OFDM modulated signal, in addition to pulse and amplitude modulated signals.

2.5 Summary

Test waveforms from current EMC standards were found to be based on a pulse modulated signal, with parameters representative of the GSM standard. However, studies on radiated susceptibility showed that test waveforms with increased complexity, such as Gaussian noise and OFDM signals yield different susceptibility thresholds. Parameters, such as the rise time, the PAPR, and the discontinuous transmissions were found to have a significant effect on EMI immunity. Furthermore, few studies have provided considerations for the design of test waveforms that are representative of the LTE standard.

3 The LTE Standard

The EMC standards reviewed in chapter 2 recommend test waveforms that are representative of GSM, but these standards do not include a test waveform for LTE. To emulate complex modulation such as OFDM, DO294C recommends using a filtered white Gaussian noise, with a high PAPR [4]. Some features of LTE standard, such as the signal edges caused by TDMA, are common with GSM. However, SC-FDMA is specific to LTE, and it is not known if it would induce EMC susceptibilities that were not present for other communication standards. An analysis of the LTE communication standard is necessary in order to design a representative test waveform. In this chapter, we will review the characteristics of the LTE standard and we will analyse the recordings of actual LTE signals.

3.1 Characteristics of the LTE standard

3.1.1 Uplink and downlink transmission

LTE is a duplex communication standard, in which both the user equipment and the base station can transmit and receive information, as shown in Fig. 3.1. For the purpose of designing EMC test waveforms, only the uplink transmission needs to be considered.

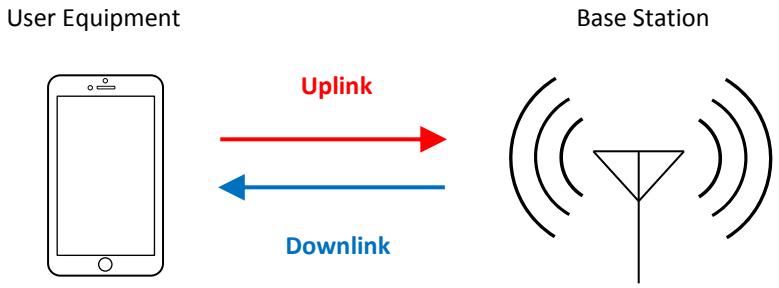

Figure 3.1: LTE uplink and downlink transmission

3.1.2 Frequency and time division duplexing

Frequency division duplexing (FDD) and time division duplexing (TDD) are two modes of duplex communication that define how the frequency channels are shared between uplink and downlink transmissions. In FDD, the uplink transmissions are always different frequency channels than the downlink transmissions; in TDD, the same frequencies channels are used, but alternating time slots are allocated for uplink and downlink transmissions. GSM use FDD only [2], but LTE uses FDD in some frequency bands and TDD in others [3]. To limit the scope of this thesis, only LTE-FDD will be considered in the design of test waveforms for LTE.

3.1.3 Frame structure

The radio frame is the structure of reference in LTE to allocate times slots to different users [3]. Although three frame structures are defined in the LTE standard, only the frame structure associated with LTE-FDD will be used. A 10 ms LTE radio frame is composed of 10 subframes of 1 ms each, as shown in Fig. 3.2. Each subframe can further be divided in two 0.5 ms LTE slots. LTE subframes are composed of either 14 symbols when the normal cyclic prefix (CP) configuration is used or 12 symbols when the extended CP configuration is used.

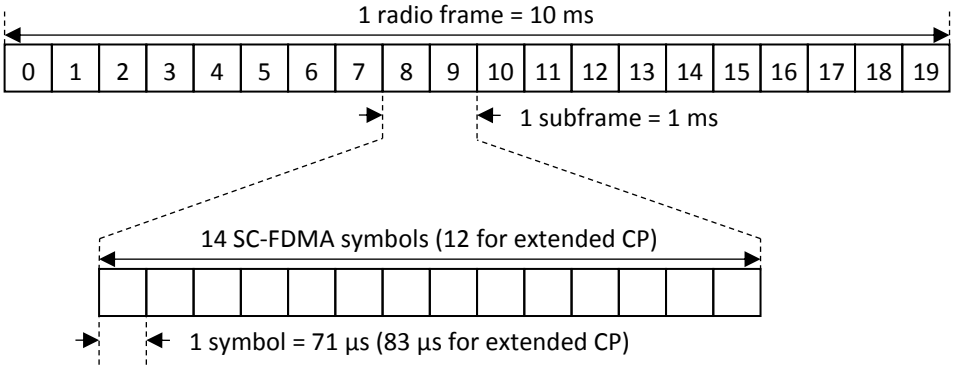

Figure 3.2: LTE frame structure type 1 [3]

3.1.4 Uplink physical channels

The LTE standard uses three different uplink physical channels to carry information blocks from the user equipment to the base station [3]:

1) The Physical Uplink Shared Channel (PUSCH): it is a transport channel used to transmit the user data. It also carries the channel quality indicator and the rank indicator to report the condition of the downlink channel to the base station.

2) Physical Uplink Control Channel (PUCCH): it is a logical channel used to transmit uplink control information. It is transmitted simultaneously with PUSCH.

3) Physical Random Access Channel (PRACH): it is a transport channel used by user equipment to access the LTE network for transmission set-up.

The PUCCH and the PRACH do not transmit user data. The transmission length of these physical channels is typically shorter than the PUSCH's: in the LTE recordings analyzed in this chapter, the PUSCH occupied significantly more transmission time than the PUCCH and the PRACH. Moreover, the transitions of power in PUCCH and PRACH were similar to those of the PUSCH. For these reasons, only the PUSCH will be used in the design of test waveforms.

Three modulations are available for the SC-FDMA symbols in the PUSCH: quadrature phase shift keying (QPSK), 16 point quadrature amplitude modulation (16QAM), and 64 point quadrature amplitude modulation (64QAM). The modulation is determined by the modulation coding scheme (MCS) index, an integer with a value interval from 0 to 28.

3.1.5 LTE frequency spectrum operating bands

The LTE standard uses a variety of frequency operating bands in order to adapt to the spectrum allocation for mobile communication in different countries [3]. LTE uses frequencies bands allocated for the GSM standard [2], with additional frequencies bands that have been allocated for mobile communications since GSM was introduced. Existing GSM and LTE frequency bands are shown in Fig. 3.3.

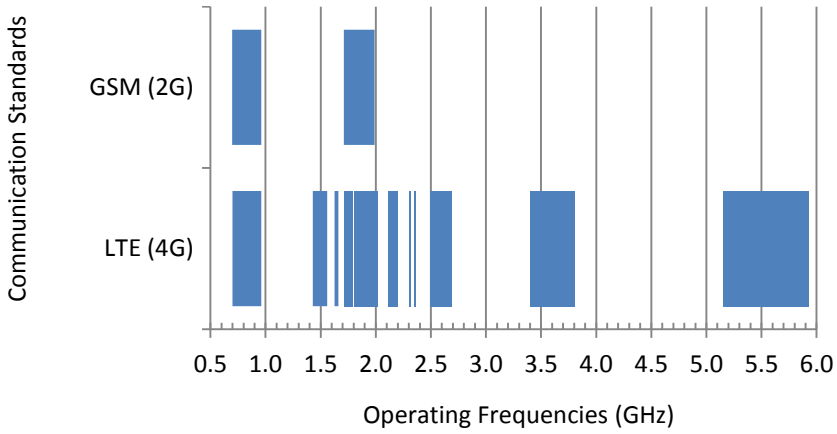

Figure 3.3: Existing GSM and LTE frequency bands [2] [3]

3.1.6 Power control classes

Power control classes define the maximum output power that can be transmitted by a device. Two power classes are used in the LTE standard [3]: power class 1 and power class 3. Power class 1, also known as high power user equipment, can only be used in LTE band 14 (788 to 798 MHz), and is limited to 31 dBm, with a tolerance of +2/-3 dB. Power class 3 is applicable to all LTE bands, and is limited to 23 dBm, with a tolerance of +2/-2 dB. Because high power user equipment is intended for public safety networks and not for consumer equipment, only power class 3 will be used in the design of test waveforms.

3.1.7 Channel and transmission bandwidths

The LTE standard [3] uses six pre-determined channel bandwidths, as listed in Table 3.1. Each channel has a maximum number of resource blocks available for transmission. The transmission bandwidth within the channel is dependent on the number of resource blocks used for transmission. Resource blocks are used in LTE to allocate the frequencies to different users within a channel.

Table 3.1: Channel and transmission bandwidth configuration for LTE [3]

Channel bandwidth [MHz]	1.4	3	5	10	15	20
Maximum number of resource blocks	6	15	25	50	75	100

Each resource block is composed of 12 subcarriers spaced at 15 kHz, for a total bandwidth of 180 kHz. An example of a LTE channel with a bandwidth of 5 MHz and with 25 allocated resource blocks is shown in Fig. 3.4.

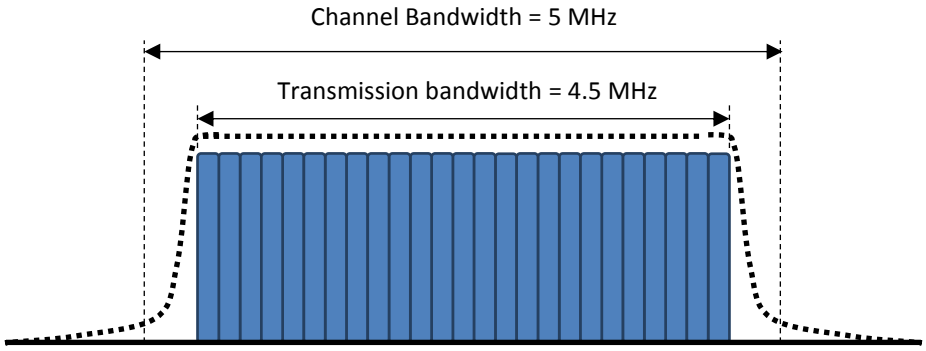

Figure 3.4: LTE channel with a bandwidth of 5 MHz [3]

3.1.8 Sounding Reference Signal

The sounding reference signal (SRS) is an optional feature of the LTE standard [3]. One SRS can be transmitted by the user equipment in the last symbol of a specific subframe to evaluate the quality of the uplink channel. The SRS scheduling can be repeated every 1, 2, 5 or 10 subframes. To prevent interference with the SRS transmitted by other user equipment, LTE devices cannot transmit during the symbol for which a SRS is scheduled, also known as SRS blanking.

3.1.9 Spectrum emission mask

The spectrum emission mask (SEM) is a measure of the maximum out-of-band emissions defined by the LTE standard [3]. The SEM limits for LTE are shown in Table 3.2. It is important to note that the power spectrum limits are given for specific out-of-band frequency intervals. Moreover, the LTE standard specifies two resolution bandwidths (RBW) for the SEM measurements in out-of-band frequency intervals: a RBW of 30 kHz for the out-of-band frequencies from 0 to 1 MHz, and a RBW of 1 MHz for the out-of-band frequencies from 1 to 25 MHz [3].

Table 3.2: SEM limits (dBm)/ Channel bandwidth [3]

Out-of-band frequencies	Power spectrum limits (dBm) / Channel Bandwidth (MHz)						Resolution bandwidth
	1.4 MHz	3 MHz	5 MHz	10 MHz	15 MHz	20 MHz	
± 0–1 MHz	-10 dBm	-13 dBm	-15 dBm	-18 dBm	-20 dBm	-21 dBm	30 kHz
± 1–2.5 MHz	-10 dBm	-10 dBm	-10 dBm	-10 dBm	-10 dBm	-10 dBm	1 MHz
± 2.5–2.8 MHz	-25 dBm	-10 dBm	-10 dBm	-10 dBm	-10 dBm	-10 dBm	1 MHz
± 2.8–5 MHz		-10 dBm	-10 dBm	-10 dBm	-10 dBm	-10 dBm	1 MHz
± 5–6 MHz		-25 dBm	-13 dBm	-13 dBm	-13 dBm	-13 dBm	1 MHz
± 6–10 MHz			-25 dBm	-13 dBm	-13 dBm	-13 dBm	1 MHz
± 10–15 MHz				-25 dBm	-13 dBm	-13 dBm	1 MHz
± 15–20 MHz					-25 dBm	-13 dBm	1 MHz
± 20–25 MHz						-25 dBm	1 MHz

3.1.10 Summary of LTE characteristics

LTE is a complex communication standard: existing EMC standards do not capture the extent of its complexity. Moreover, testing for each LTE parameter would lead to a large number of combinations. It was decided to limit the scope of this thesis

to LTE waveforms with frequency division duplexing (FDD), using the Physical Uplink Shared Channel (PUSCH). LTE signals with such parameters will be analyzed in Section 3.2 in order to design representative test waveforms.

3.2 Analysis of LTE signal recordings

Analysis of actual LTE signals can be useful for understanding the LTE standard. In this section, the methodology for recording the LTE signals will be described, followed by a spectrum analysis, and a PAPR analysis.

3.2.1 LTE signal recording

LTE signals from two mobile devices were recorded using an antenna and a vector signal analyzer (VSA), as shown in Fig. 3.5. The antenna used was Aaronia's 60250 wideband log-periodic, with a gain of 5 dBi and a frequency range from 680 MHz to 25 GHz. Keysight's M9393A vector signal analyzer, with a frequency range from 1 MHz to 3 GHz was used to record the signal.

Sixteen different LTE signals were captured using this setup. Two mobile devices using different mobile communications providers were used to transmit the signals. The transmitting conditions were created by uploading different sized files to an email server or to a data cloud in order to maximize the uplink channel throughput. Keysight's 89600 VSA software was used to demodulate the carrier-modulated signals to baseband samples that were then stored in a file. Different sampling frequencies were chosen to minimize the file sizes without compromising the data. Three signals with unique properties were retained for further analysis.

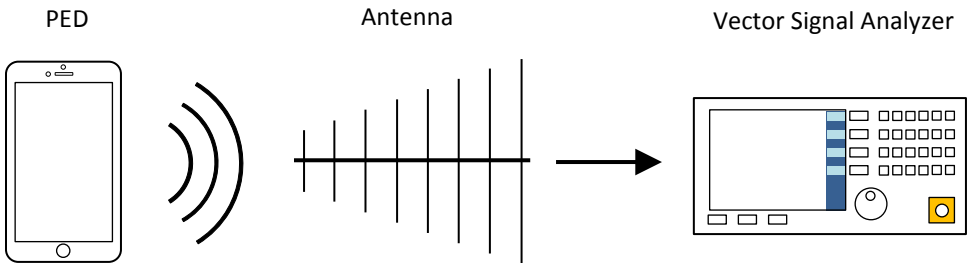

Figure 3.5: LTE signals recording setup

3.2.2 Spectrum analysis

The first LTE signal was recorded from a BlackBerry model Q10 mobile phone, operating on the Rogers wireless network. The phone was used to upload a large data file on an email server in order to create a high throughput transmission. The center frequency for the LTE signal was 707 MHz, which corresponds to the LTE frequency band 12, also known a seven hundred megahertz band. A sampling frequency of 6.4 MHz was used for the VSA recording. A total of 3.2 million complex samples from the original recording were used for analysis, resulting in a length of 500 ms (1000 LTE slots).

MathWorks' Matlab release 2016a software was used to analyse the LTE signals. The first step of the analysis was to display a spectrogram of the signal to observe the signal characteristics. Matlab's spectrogram function uses the short time Fourier transform to create a graph of the signal's power spectral density. The spectrogram of the samples within the first LTE signal is shown in Fig. 3.6.

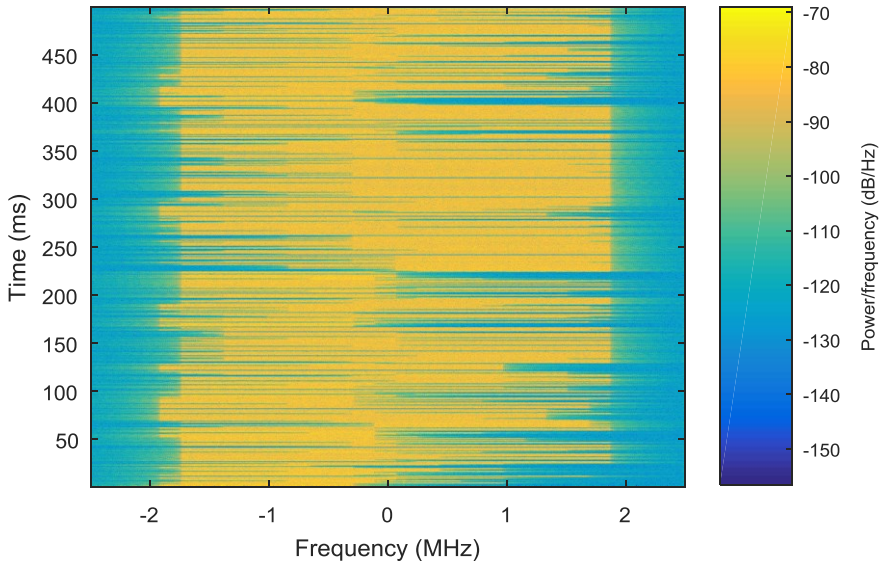

Figure 3.6: First LTE signal – spectrogram of 50 LTE frames (500 ms)

A window size of 4096 samples was used to display a spectrogram of the whole signal length. By observation of the spectrogram, it was deduced that the first LTE signal had a channel bandwidth of 5 MHz. Signals were transmitted in all the recorded frames, however the resource blocks allocation varied significantly. To inspect the signal in more detail, a spectrogram of one LTE frame (10 ms) within the first LTE signal was plotted, as shown in Fig. 3.7.

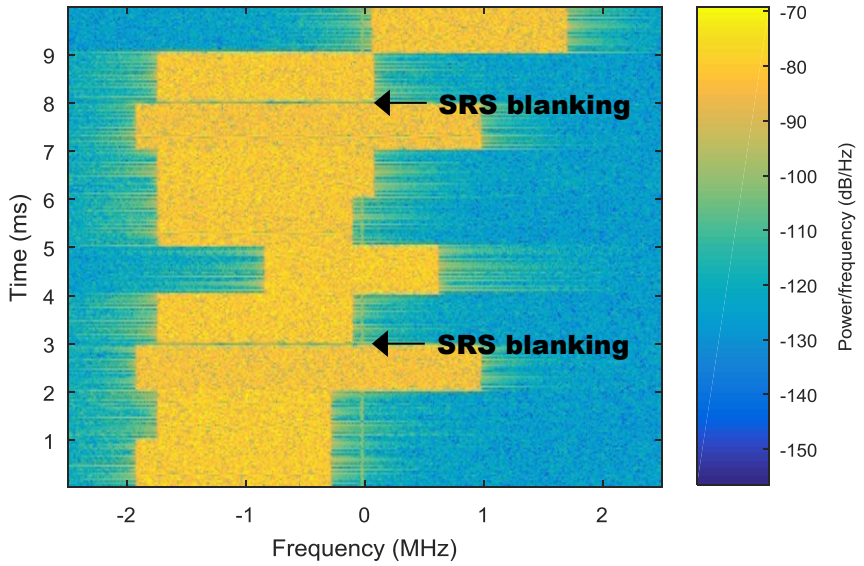

Figure 3.7: First LTE signal – spectrogram of one LTE frame (10 ms)

The bandwidth of the LTE signal was constant within each subframe, and the resource block allocation did not follow a particular pattern. The recorded signal was identified as the Physical Uplink Shared Channel (PUSCH), for this channel was used to transmit data. However, this spectrogram gave no indication on the type of Modulation Coding Scheme (MCS) that was used. The signal within this frame was almost continuous, with the exception of the SRS blanking during the last SC-FDMA symbols of the third and eight subframes not being transmitted. As described in Section 3.1.8, the SRS scheduling can be repeated every 1, 2, 5 or 10 subframes. In this case, the SRS blanking uses a configuration period of five subframes (5 ms). To further inspect the signal, a spectrogram of the third subframe within the LTE frame displayed earlier was plotted, as shown in Fig. 3.8.

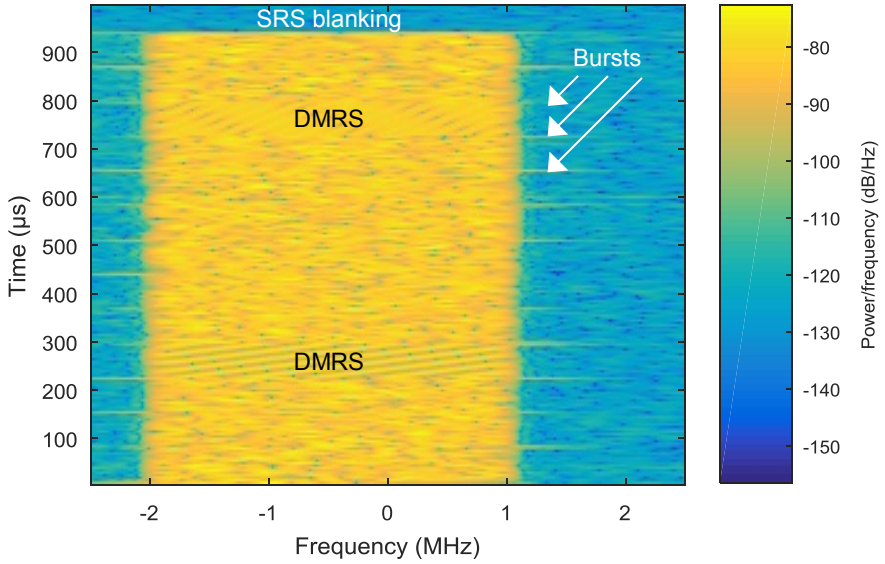

Figure 3.8: First LTE signal – Spectrogram of one LTE subframe (1 ms)

Transitions between SC-FDMA symbols could be seen in the form of repeating periodic bursts on each side of the main frequency band. These outbursts correspond to a short emission of out-of-band energy caused by the rapid voltage change between two different SC-FDMA symbols. These outbursts did not cause the power spectrum to exceed the SEM. The last symbol of the LTE subframe was not transmitted, which corresponds to the SRS blanking described earlier. The power spectral density within the subframe was relatively constant. Oblique patterns in the fourth and eleventh SC-FDMA symbols within this LTE subframe are evident in Fig. 3.9. These oblique patterns can be explained by the Zadoff-Chu sequences, which correspond to the demodulation reference signals (DMRS) in the LTE standard [3].

3.2.3 PAPR analysis

The PAPR for all of the LTE slots was computed by dividing the maximum of the absolute value by the root mean squared (RMS) value, as expressed in (3.1).

$$PAPR = \frac{|x|_{max}}{x_{RMS}} \tag{3.1}$$

The LTE slot was chosen as the standard length for all PAPR analysis, for it is the smallest LTE element with a specified length (0.5 ms). The number of samples used to compute the PAPR had a direct effect on the PAPR: increasing the number of samples yields a higher PAPR, for there is a higher probability of encountering a large maximum value within that period.

Matlab's occupied bandwidth (OBW) function was used to compute the frequency bandwidth corresponding to 99% of the power spectrum for each LTE slot. The PAPR and the OBW values were plotted, as shown in Fig. 3.9. The OBW data formed tight groups around certain values, which corresponds to the number of resource blocks used for transmission in the LTE signal.

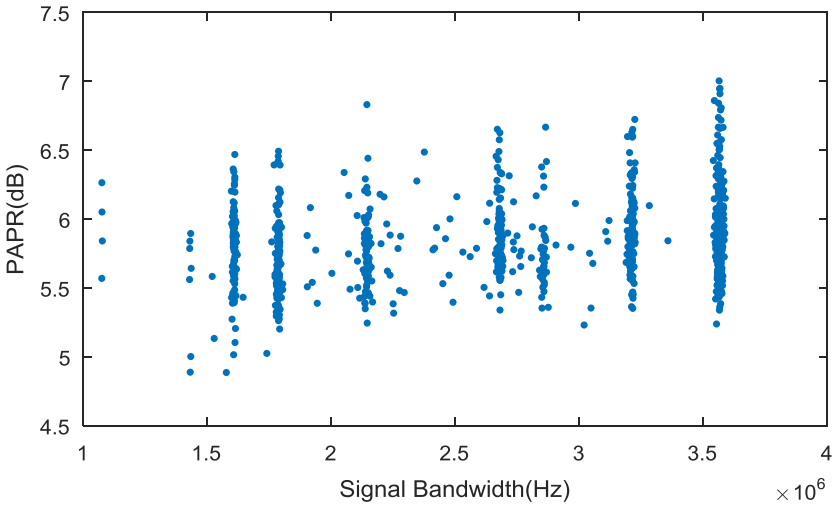

Figure 3.9: First LTE signal – PAPR and OBW data

The PAPR computed for the LTE slots were found to be randomly distributed: the probability density function (PDF) of the PAPR values followed a normal distribution. Matlab's normfit function was used to estimate the mean and the standard deviation of the PAPR values. The statistical analysis estimated a mean of 5.85 dB, and a standard deviation of 0.31 dB. Matlab's histfit function was used to plot a histogram of the PAPR values and a trace of the normal PDF, as shown in Fig. 3.10. The histogram was in good agreement with the trace of the normal PDF.

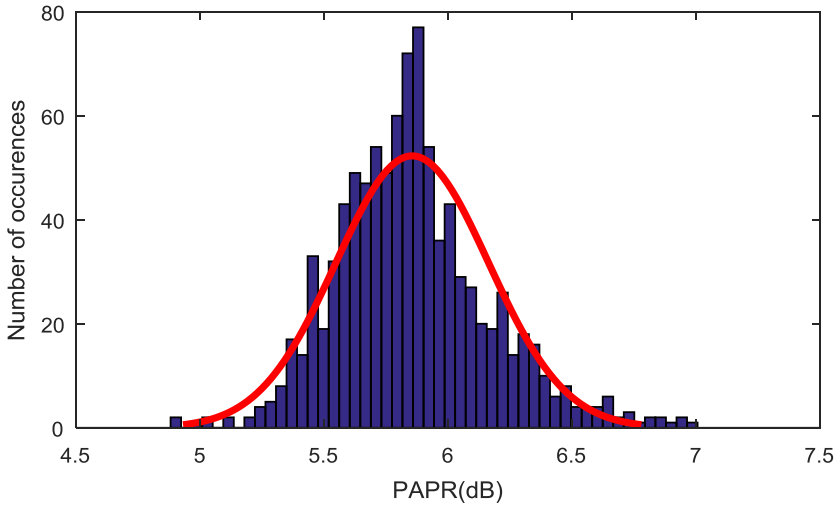

Figure 3.10: First LTE signal – PAPR histogram and normal distribution

3.2.4 Second LTE signal

For the purpose of evaluating the effect of the slot bandwidth, a second LTE signal was recorded from an Apple iPhone model A1549, operating on the Bell wireless network. The phone was used to upload a large data file on a cloud storage server. The LTE signal's center frequency was 712.5 MHz, which corresponds to the LTE frequency band 12. A sampling frequency of 25.6 MHz was used for recording the second LTE signal, which corresponds to four times the sampling frequency of the

first LTE signal. A total of 12.85 million complex samples were used for analysis, resulting in 500 ms (1000 LTE slots). The spectrogram of one LTE frame (10 ms) within the second LTE signal is shown in Fig. 3.11.

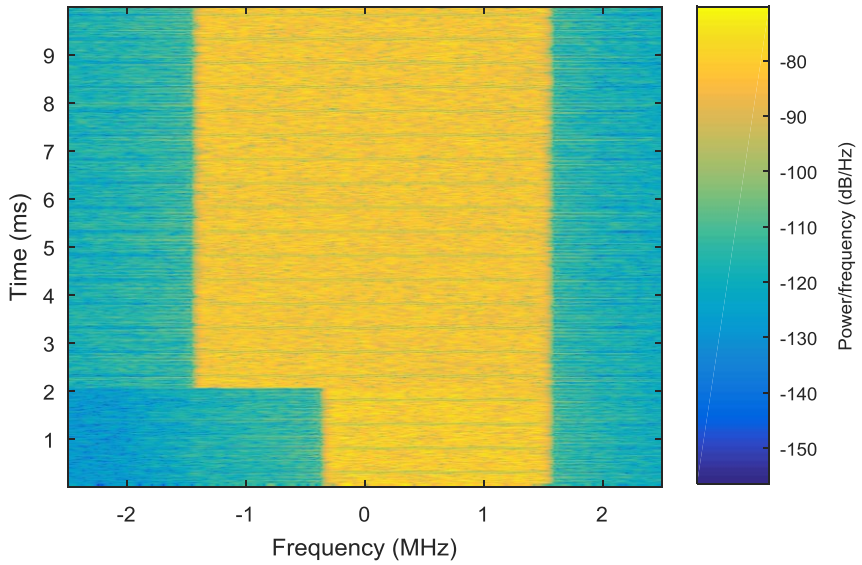

Figure 3.11: Second LTE signal – spectrogram of one LTE frame (10 ms)

The resource block allocation had a specific subframe pattern: the first two subframes (2 ms) of each LTE frame had a smaller bandwidth, while the remaining eight subframes (8 ms) had a larger bandwidth. This subframe pattern was repeated for all LTE frames within the second LTE signal. The signal within these frames was continuous and no occurrences of SRS blanking were observed.

The PAPR and OBW values for each LTE slot were plotted on a graph shown in Fig. 3.12. The OBW data mostly formed tight groups around two values. A first group of data had an OBW of 1.8 MHz, which corresponds to 10 resource blocks. A second group of data had an OBW of 2.9 MHz, which corresponds to 16 resource blocks. These values are consistent with the bandwidth of the subframe pattern described earlier.

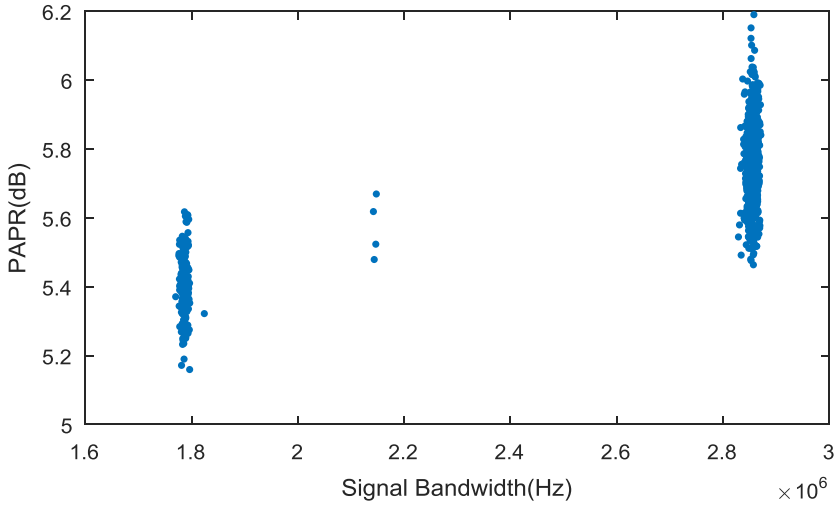

Figure 3.12: Second LTE signal – PAPR and OBW data

Histograms of both groupings were plotted, as shown in Fig. 3.13. A mean of 5.40 dB and a standard deviation of 0.09 dB were estimated for the slots with an OBW of 1.8 MHz, whereas a mean of 5.76 dB and a standard deviation of 0.11 dB were estimated for the slots with an OBW of 2.9 MHz.

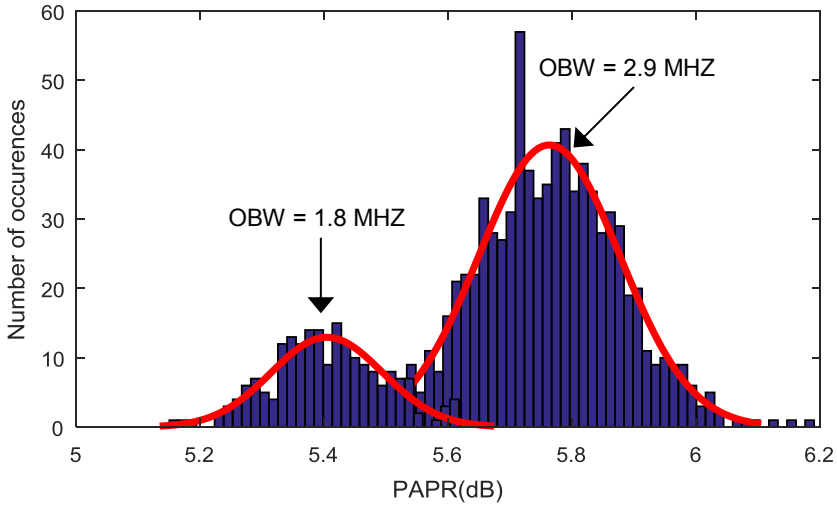

Figure 3.13: Second LTE signal – PAPR histograms and normal distributions

Both histograms were in good agreement to the traces of the normal PDFs. It was observed that the OBW of the LTE slots had a significant effect on the PAPR: an increase in the OBW led to higher PAPR. This can be explained by the fact that when the signal's frequency is increased, there is a higher probability of encountering a large maximum value within that period.

3.2.5 Third LTE signal

For the purpose of evaluating the effect of the MCS index on the PAPR, a third LTE signal was recorded in similar conditions that of the second LTE signal: the same mobile phone was used to upload a large data file on a cloud storage server. The LTE signal had a center frequency of 1877.5 MHz, which corresponds to the LTE frequency band 2, also known as the personal communications service band. A sampling frequency of 51.2 MHz, and 12.85 million complex samples were used for analysis, resulting in a total length of 500 ms (1000 LTE slots). The spectrogram of one LTE frame within the third LTE signal is shown in Fig. 3.14.

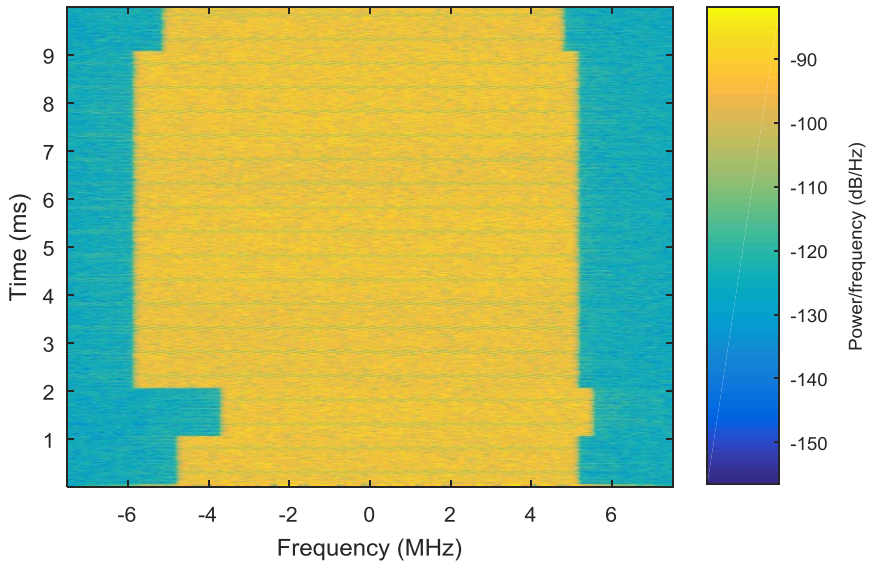

Figure 3.14: Third LTE signal – spectrogram of one LTE frame (10 ms)

The PAPR and OBW values for each LTE slot were plotted on a graph shown in Fig. 3.15. Similar to the second LTE signal, the measured OBW of the LTE slots data formed tight groups around two values. A first group of slots had an OBW of 9.7 MHz, which corresponds to 54 resource blocks. A second data group had an OBW of 10.7 MHz, which corresponds to 60 resource blocks. However, contrary to the second LTE signal, the OBW was not used to discriminate the PAPR data.

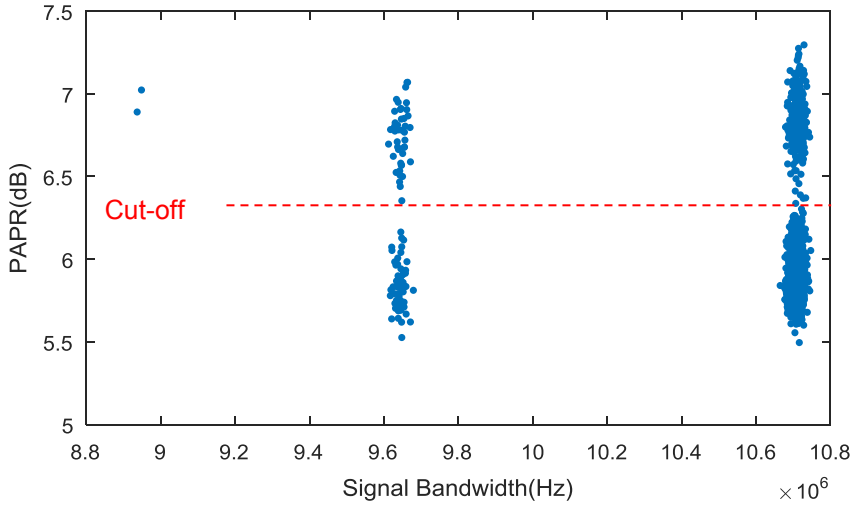

Figure 3.15: Third LTE signal – PAPR and OBW data

The PAPR of the LTE slots within the third signal had significantly higher variance than the PAPR of the LTE slots within the previous signals, even for the LTE slots that had the same OBW. To verify if the variance was caused by the presence of two sets of independent variables, the data points were divided in two groups using a cut-off PAPR of 6.34 dB. LTE slots with a PAPR less than 6.34 dB had a mean PAPR of 5.89 dB, and a standard deviation of 0.15 dB. LTE slots with a PAPR higher than 6.34 dB had a mean PAPR of 6.84 dB, and a standard deviation of 0.18 dB. The difference between the mean PAPR of the two data sets (0.95 dB) was more than five times the largest standard deviation (0.18 dB) for a data set. It can therefore be deducted that two sets of independent variables with

different signal parameters are present. It is hypothesized that the modulation coding scheme (MCS) varied within the LTE signal, and that it had an effect on the measured PAPR. For example, some LTE slots could have a lower MCS index associated with a QPSK modulation, while other LTE slots could have a higher MCS index associated with a 16QAM modulation.

Histograms of the PAPR data from the third LTE signal and traces of the normal PDF were plotted, as shown in Fig. 3.16. Both histograms were in good agreement to the traces of the normal PDFs.

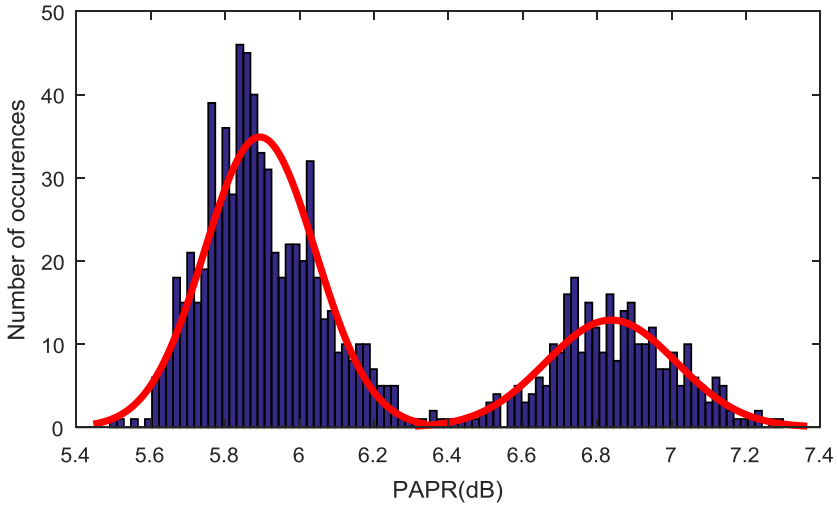

Figure 3.16: Third LTE signal – PAPR histograms and normal distributions

3.3 Summary

The analysis showed that the PAPR of the LTE signals were randomly distributed, and in good agreement to normal PDF. It was found that the OBW and the PAPR measurement of a LTE signal were not independent, that oversampling a signal did not affect significantly its measured PAPR. Moreover, it was hypothesized that the MCS index has a significant effect on the PAPR of a LTE signal.

4 Test waveform design

Chapter 3 described the complexity of the LTE standard. This chapter will cover the design of test waveforms that are suitable for radiated susceptibility testing. To ensure that each test waveform is representative of the LTE standard, their power spectrum will be compared to the spectrum emission mask (SEM). The PAPR of the test waveforms will also be analyzed, in order to select the parameters that could yield the most significant results during radiated susceptibility testing.

4.1 Methodology and considerations

DO294C provided some guidance for the design of test waveforms of complex communication standards such as LTE [4]. It claimed that the highest interference threat is linked to signals with pulse modulation: the fast change in amplitude was alleged to have the greatest effect on the susceptibility of the victims. Amplitude changes caused by digital modulation schemes such as QAM were said to increase the susceptibility of victim systems, but with less effect than pulse modulation. DO294C argued that frequency and phase changes caused by digital modulation do not have a significant effect on the susceptibility, suggesting that phase shift keying can be modeled by a continuous wave. Moreover, DO294C claimed that the waveform duty cycle does not have a significant effect on the susceptibility, and that the effect of the peak power is more significant than that of the signal energy.

Previous studies on radiated susceptibility also provided insights for the design of test waveforms. The study performed at NTT DoCoMo found that variations in the PAPR did not have a significant effect on the susceptibility [10]. However, this observation has not been replicated. It is suspected that a high PAPR can induce a higher susceptibility on victim systems, but that to measure its effect, the test waveforms parameters must be controlled using an appropriate methodology.

4.1.1 Parameter reduction process

In the EMC community, simple test waveforms are preferred over complex test waveforms, to obtain reproducible results during radiated susceptibility testing. In order to reduce the complexity of the test waveforms, a parameter reduction process was developed: characteristics of the LTE waveform were gradually removed, so that each signal had less complexity than the previous one. The choice of test waveforms that resulted from this process is shown in Fig. 4.1.

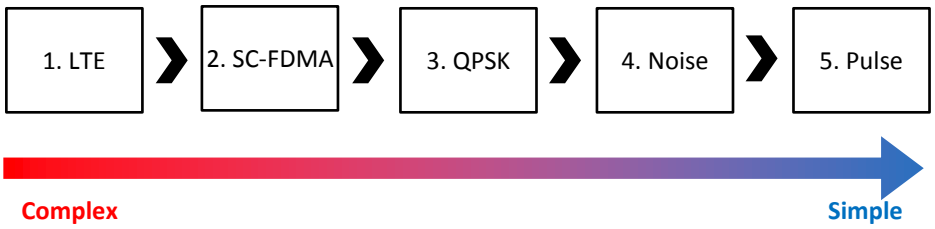

Figure 4.1: Parameter reduction process for the choice of test waveforms

The first waveform chosen for parameter reduction is an actual LTE signal with the PUSCH format, including SC-FDMA modulation, DMRS and SRS blanking. The second waveform is a continuous signal with SC-FDMA modulation: the parameters used in the SC-FDMA modulated waveform were chosen to emulate the characteristics of the LTE waveforms, except for DMRS and SRS blanking. The third and the fourth waveforms used similar root raised cosine (RRC) filters to conform to the SEM: the third waveform is a filtered QPSK modulated signal; the fourth waveform is a filtered noise signal. The fifth waveform is a pulse modulated signal: the pulse repetition frequency and the duty factor were chosen to emulate the SRS blanking; the rising and falling edges lengths were selected to conform to the SEM. To compare the frequency response of the test waveforms to the SEM, all waveforms were normalized to 23 dBm, the maximum power output for LTE power class 3 devices [3].

4.1.2 Spectrum emission mask adjustments

As described in Section 3.1.9, two different resolution bandwidths (RBW) are specified by the LTE standard: a RBW of 30 kHz for the out-of-band frequencies from 0 to 1 MHz, and a RBW of 1 MHz for the out-of-band frequencies from 1 to 25 MHz [3]. However, it would be more convenient to compare the power spectrum of the test waveforms to SEM limits using a single RBW. Using a RBW of 1 MHz yields higher power spectrum values than using for 30 kHz, because more power is integrated at each frequency component.

The SEM limits were adjusted to account for the difference in the RBW. The adjustment factor was computed using the common logarithm of the ratio of a RBW of 1 MHz to a RBW of 30 kHz, multiplied by ten, as expressed in (4.1).

$$Adjustment\ factor = 10\log_{10}\left(\frac{1\ \text{MHz}}{30\ \text{kHz}}\right) = 15.2\ \text{dB} \tag{4.1}$$

The adjustment factor of 15.2 dB was added to the SEM limits with a RBW of 30 kHz, and subtracted to the SEM limits with a RBW of 1 MHz, to obtain the adjusted SEM limits corresponding to different RBW values. The adjusted SEM limits were calculated for each LTE channel bandwidth. Those for a LTE channel bandwidth of 20 MHz are listed in Table 4.1.

Table 4.1: Adjusted SEM limits for a LTE channel bandwidth of 20 MHz

Out-of-band frequencies	Original SEM limits	Original RBW	Adjusted SEM limits	
			RBW 30 kHz	RBW 1 MHz
± 0–1 MHz	-21 dBm	30 kHz	-21 dBm	-5.8 dBm
± 1–5 MHz	-10 dBm	1 MHz	-25.2 dBm	-10 dBm
± 5–20 MHz	-13 dBm	1 MHz	-28.2 dBm	-13 dBm
± 20–25 MHz	-25 dBm	1 MHz	-40.2 dBm	-25 dBm

4.2 LTE waveform design

As discussed in Section 3.1.4, the PUSCH format was chosen for the design of test waveforms. In the following sections, the waveform parameters will be chosen to create a signal that is representative of the LTE communication standard.

4.2.1 SystemVue signal generator for LTE

Keysight's SystemVue, release 2015.01, software was used to generate the LTE signals with a 20 MHz channel bandwidth. Four patterned data sources were connected to a baseband LTE source (release 8.9). SRS blanking periods were allocated during subframe 3 and 8. For the purpose of spectrum shaping, a RRC filter with a roll-off factor of 0.22 was chosen. An oscillator with a carrier frequency and a complex signal to envelope signal converter were used to modulate the carrier. A signal downloader for Keysight's M9381A vector signal generator (VSG) was used to save to a binary file, and a data sink was used to record the signals to a comma-separated values (CSV) file for analysis in Matlab. The design schematic of the LTE signal generator is shown in Fig. 4.2.

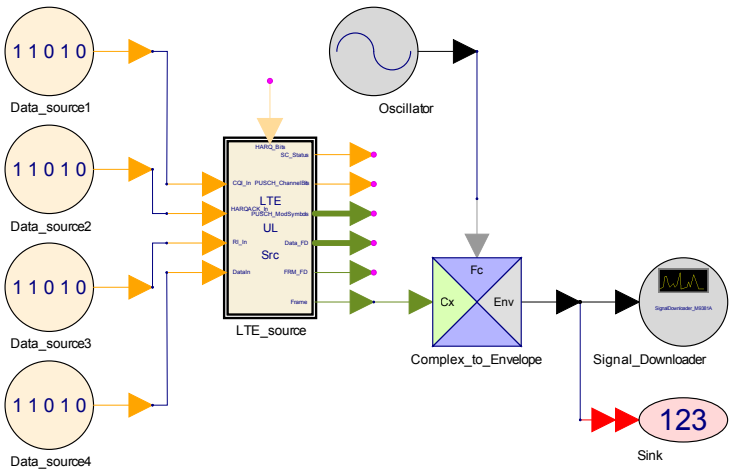

Figure 4.2: Design schematic of the LTE signal generator

4.2.2 Spectrum analysis of the LTE signals

Matlab's spectrogram and periodogram functions were used to estimate the PSD of the test waveforms. The spectrogram of the third subframe within a LTE signal with a channel bandwidth of 20 MHz is shown in Fig. 4.3. A Hann window, a window length of 512 samples, and a sampling frequency of 30.72 MHz were used.

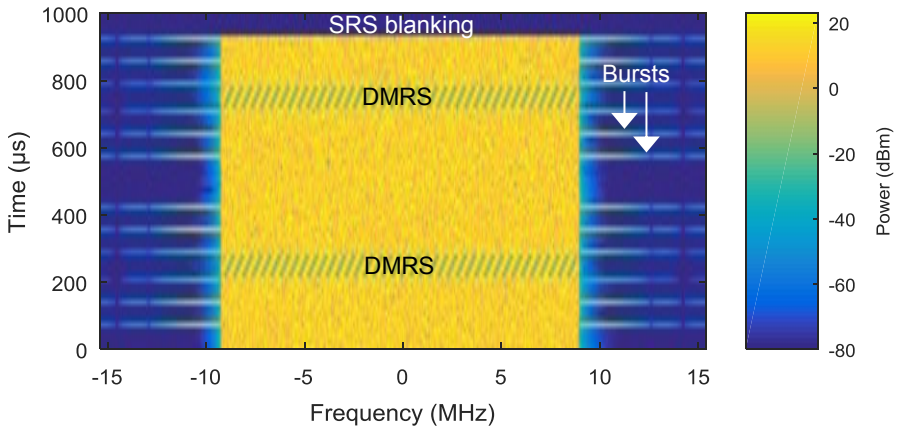

Figure 4.3: Spectrogram of the third LTE subframe (1 ms)

Similar to the spectrogram of the LTE recording in Fig. 3.8, the transitions between each SC-FDMA symbol were seen in the form of periodic bursts. The out-of-band bursts were attenuated by the RRC filter used for spectrum shaping. The last symbol of the LTE subframe was not transmitted, due to the SRS blanking. Each blanking period created a falling edge and a rising edge within the LTE signal. A demodulation reference signals (DMRS) was allocated in the fourth and eleventh SC-FDMA symbols, and was characterized by the oblique patterns.

Matlab's periodogram function was used to compare the power spectrum of the LTE signals to the SEM limits. A window length of 1024 samples was used, resulting in a RBW of 30 kHz. . The samples of the LTE signal were chosen to include a rising edge associated with the end of the SRS blanking period. The

complex magnitude of the 1024 LTE samples was plotted, as shown in Fig. 4.4. The LTE signal had a peak magnitude of 7.23 V, resulting in a PAPR of 7.2 dB.

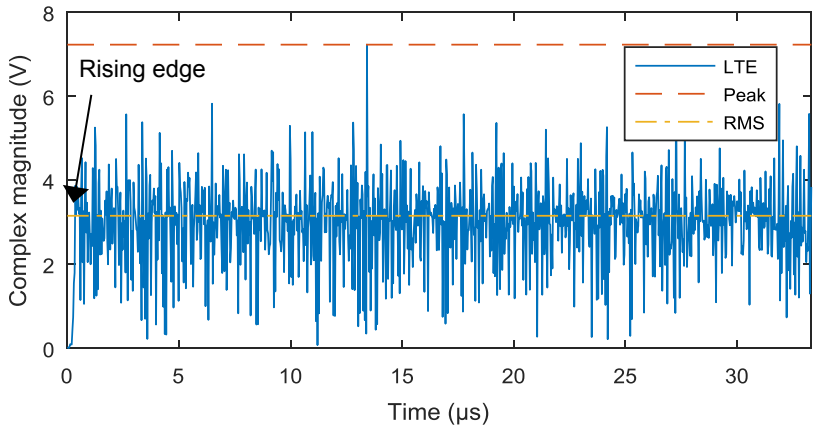

Figure 4.4: Complex magnitude of the LTE signal for spectrum analysis

A rectangular window function was used for the periodogram. The power spectrum estimate of the LTE signal was found to be lower than the SEM limits adjusted for a RBW of 30 kHz, as shown in Fig. 4.5.

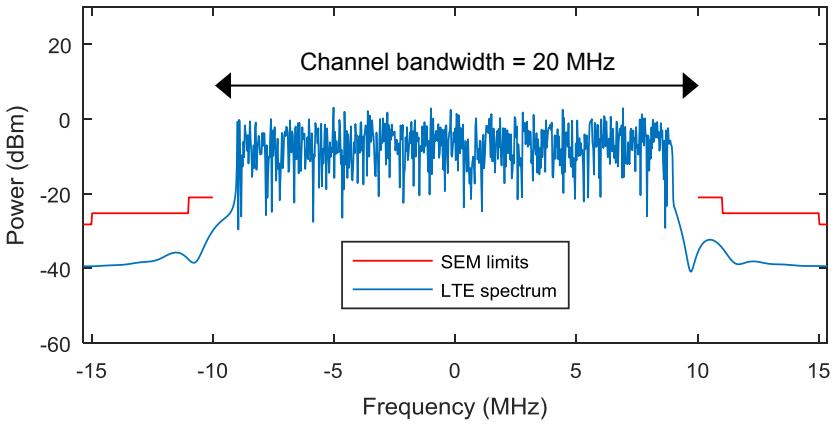

Figure 4.5: Spectrum of LTE and SEM limits, RBW of 30 kHz

A periodogram was plotted to estimate the power spectrum with a RBW of 1 MHz. The power spectrum estimate of the LTE signal using a rectangular

window was found to be exceeding the SEM limits adjusted for a RBW of 1 MHz. The power spectrum estimate using a Hann window was found to be lower the SEM limits adjusted for a RBW of 1 MHz, as shown in Fig. 4.6. Matlab's enbw function was used to calculate the equivalent noise bandwidth of the signal. Using a Hann window with a length of 47 samples yielded a bandwidth of 1 MHz.

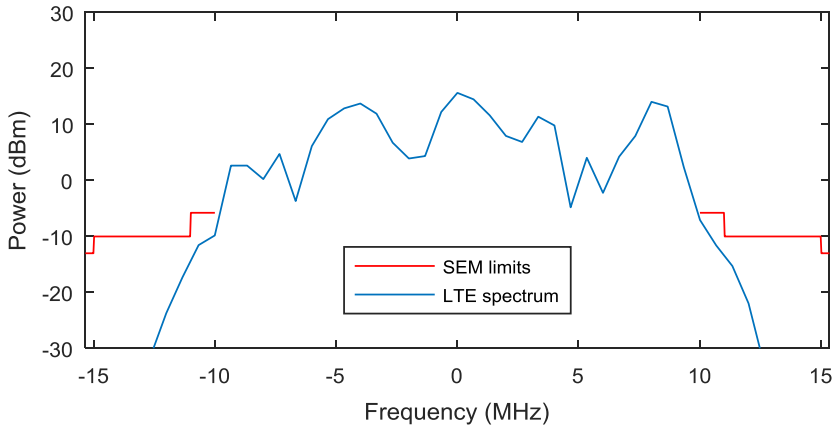

Figure 4.6: Spectrum of LTE and SEM limits, RBW of 1 MHz

4.2.3 PAPR analysis of the LTE signals

As discussed in chapter 3, the modulation coding scheme is suspected to have an effect on the PAPR. To evaluate the effect of the MCS index on the PAPR, two LTE waveforms were generated: one with a MCS index of 1, using QPSK symbol mapping, and another with a MCS index of 28, using 64-QAM mapping. Matlab's complementary cumulative distribution function (CCDF) system object was used to measure the PAPR of the LTE waveforms, as shown in Fig 4.7.

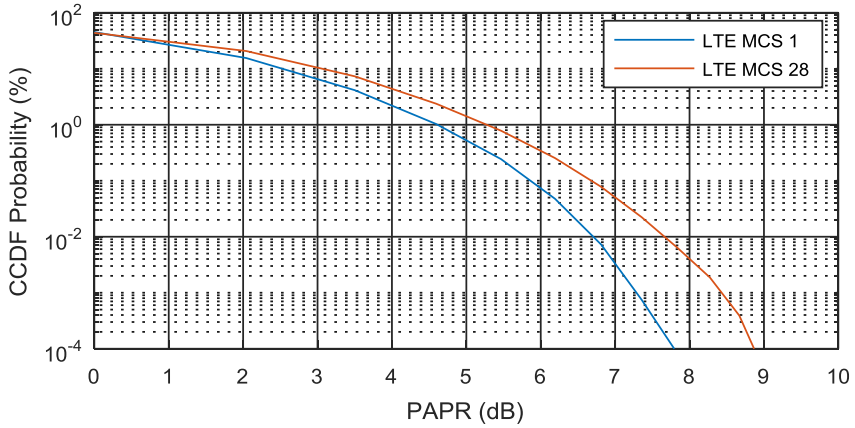

Figure 4.7: PAPR of LTE signals with MCS 1 and MCS 28

The PAPR of LTE with a MCS index of 1 was lower than the PAPR of LTE with a MCS index of 28. This observation validates the hypothesis made in Section 3.2.4 that the MCS index has a significant effect on the PAPR of a LTE signal. LTE with a MCS of 1 had a PAPR of 7.7 dB for a CCDF probability of 0.0001%, which is equal to the PAPR of the LTE release 8 signals used in the study performed at NTT DoCoMo research laboratories [10].

4.3 SC-FDMA waveform design

SC-FDMA is similar to OFDM, in that the channel bandwidth is mapped into subcarriers, before inserting the cyclic prefix. However, SC-FDMA converts the data using a FFT before the subcarriers are mapped, as shown in Fig. 4.8.

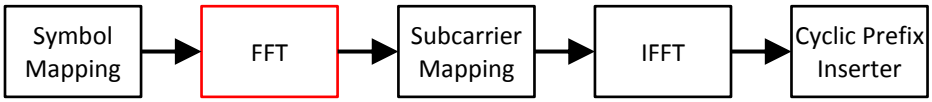

Figure 4.8: Block diagram of the SC-FDMA modulator

4.3.1 Spectrum analysis of the SC-FDMA signals

Matlab's OFDM modulator was used to generate the SC-FDMA waveforms. The resulting SC-FDMA waveforms were similar to the LTE, except for DMRS, SRS blanking and spectrum shaping filters. A spectrogram was plotted for 14 SC-FDMA symbols with a bandwidth of 20 MHz, as shown in Fig. 4.10. As for LTE, a Hann window of 512 samples, and a sampling frequency of 30.72 MHz were used.

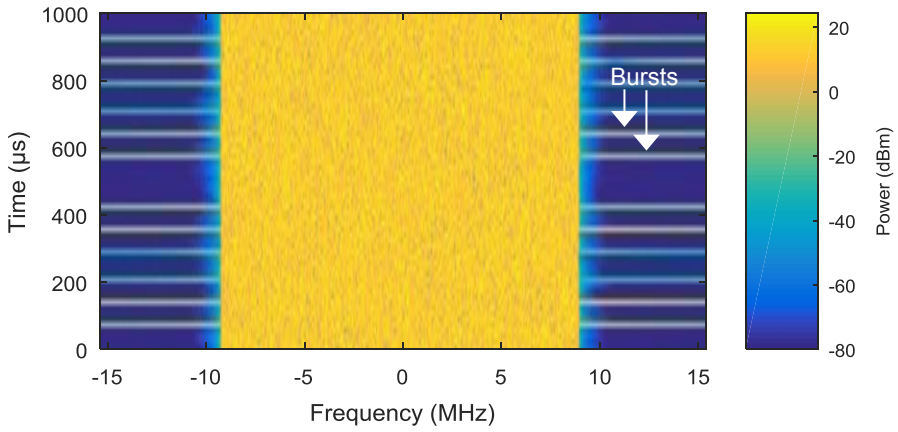

Figure 4.9: Spectrogram of 14 SC-FDMA symbols (1 ms)

The bandwidth of the SC-FDMA signal was constant within the subframe. Similar to the LTE signal, the transitions between each SC-FDMA symbol were seen in the form of periodic bursts. However, due to the lack of a spectrum shaping filter, the bursts of the SC-FDMA signal were not attenuated.

Matlab's periodogram function was used to compare the power spectrum of the SC-FDMA signals to the SEM limits adjusted to with a RBW of 30 kHz. 1024 samples within the SC-FDMA signal were chosen, including a transition between two symbols. The complex magnitude of the 1024 SC-FDMA samples is shown in Fig. 4.10. The peak amplitude within the 1024 samples was 6 V, resulting in a PAPR of 5.6 dB.

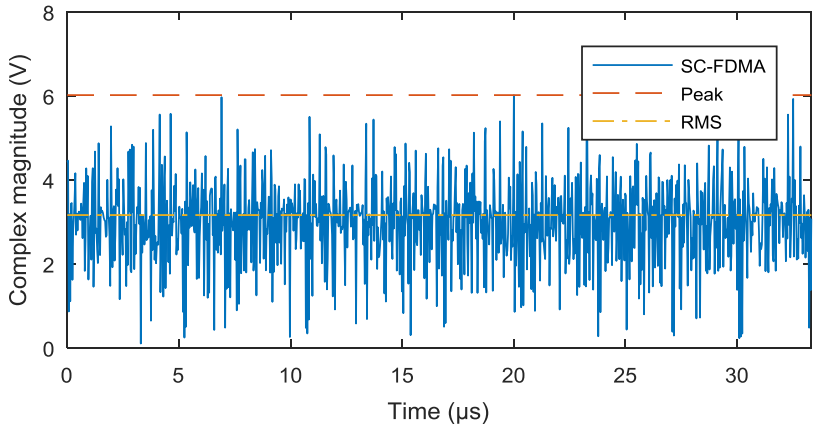

Figure 4.10: Complex magnitude of 1024 samples within the SC-FDMA signal

A rectangular window function was used for the power spectrum estimate with a RBW of 30 kHz. The spectrum of the SC-FDMA signal was found to be lower than the SEM limits, as shown in Fig. 4.11. The spectrum within the channel band was very similar to that of the LTE. However, the out-of-band spectrum of the SC-FDMA signal had a high power than the out-of-band spectrum of LTE, due to the lack of a shaping filter.

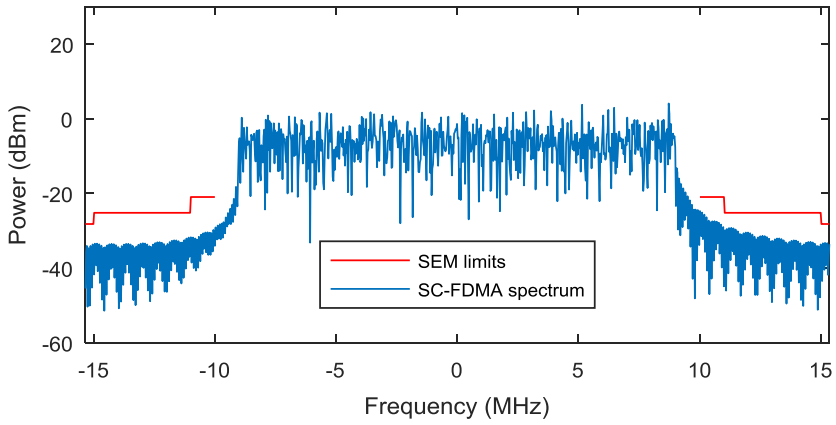

Figure 4.11: Spectrum of SC-FDMA and SEM limits, RBW of 30 kHz

Another periodogram with a Hann window and a length of 47 samples was used to estimate the power spectrum of SC-FDMA. The power spectrum was found to exceeding the SEM limits adjusted for a RBW of 1 MHz, as shown in Fig. 4.12.

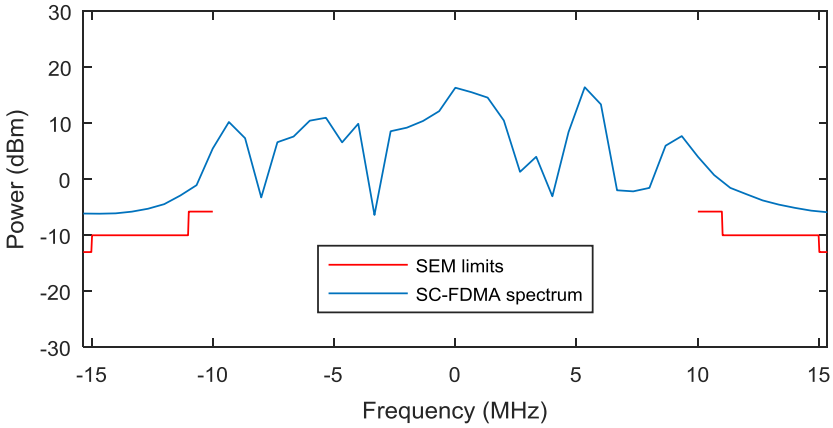

Figure 4.12: Spectrum of SC-FDMA and SEM limits, RBW of 1 MHz

The role of the spectrum shaping filter in the LTE signal generator is to attenuate the out-of-band frequencies. The lack of a spectrum shaping filter in the design of the SC-FDMA signal caused the power spectrum of the transitions between two symbols to exceed the SEM limits adjusted for a RBW of 1 MHz.

4.3.2 PAPR of the SC-FDMA signals

To evaluate the PAPR and the CCDF probabilities of SC-FDMA waveforms, two SC-FDMA signals were generated: one with QPSK symbol mapping, and another with 64-QAM symbol mapping. The PAPR measurements of the SC-FDMA signals were plotted and compared to the LTE signals, as shown in Fig 4.13.

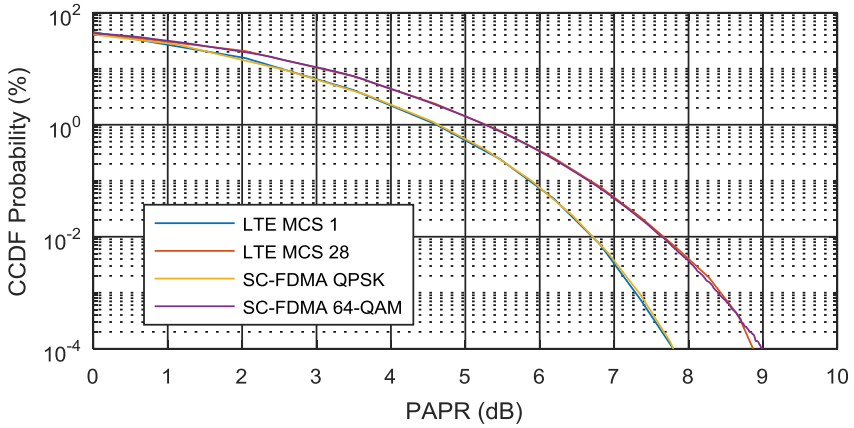

Figure 4.13: PAPR of LTE and SC-FDMA signals

The PAPR of the SC-FDMA waveform with QPSK and 64-QAM symbol mapping were respectively equivalent to the PAPR of the LTE waveform with MCS indexes of 1 and 28. It can be concluded that that DMRS, the SRS blanking, and the spectrum shaping filters that were present in the LTE signals, but absent in the SC-FDMA signals, did not have a significant effect on the PAPR. However, removing the SRS blanking period from LTE removes a significant source of amplitude variation in the test waveform, which is not measured in the PAPR analysis of the SC-FDMA waveform.

4.4 Filtered QPSK waveform design

Quadrature phase shift keying (QPSK) is a type of digital phase modulation, where symbols are mapped on a carrier using four different phases [13]. QPSK is similar to GMSK used in the GSM standard. Unfiltered QPSK signals have constant amplitude: DO294C proposes that they can be modelled by continuous waveforms [4]. Yet, filtering a QPSK signal can introduce magnitude variations. In this section, design parameters for a filtered QPSK signal will be proposed.

4.4.1 RRC filter design

Root raised cosine (RRC) filters were chosen to limit the bandwidth of the QPSK waveforms, for they are commonly used in digital communications [13]. The RRC filter's pass bandwidth is controlled by the number of samples used in the filter, also known as filter span, and the upsampling factor. An upsampling factor of 2 samples per symbol was used to create a RRC filter with a pass bandwidth of approximately half the sampling frequency. The excess bandwidth is set by the roll-off factor (beta). Matlab's rcosdesign function was used to conceive a RRC filter with a span of 6 samples and a roll-off factor of 0.22. The RRC filter introduced a time delay, that was measured using Matlab's grpdelay function, and compensated for.

Matlab's pskmod function was used to generate a QPSK signal. The QPSK signal was filtered using the RRC filter. The real parts of the unfiltered and filtered QPSK signals were plotted, as shown in Fig. 4.14: the red trace is the unfiltered signal, and the blue trace is the filtered signal. The trace of the filtered signal followed the trace of the unfiltered signal.

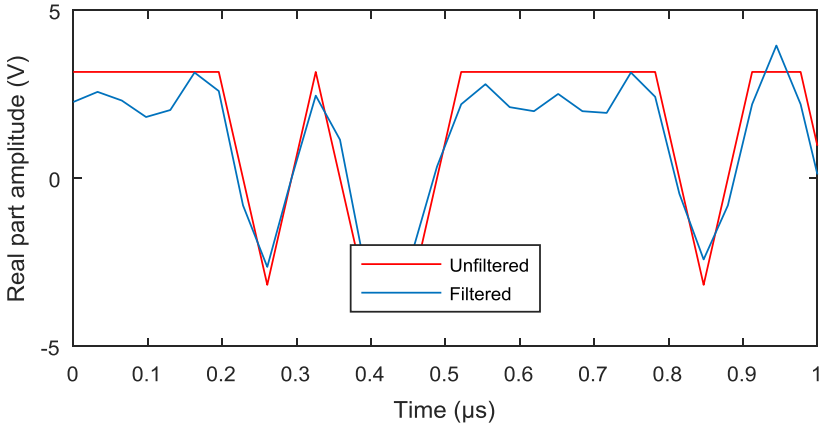

Figure 4.14: Real parts amplitude of unfiltered and filtered QPSK signals

4.4.2 Spectrum of the filtered QPSK signals

The filtered QPSK signal was normalized to a power of 23 dBm, and its spectrogram was plotted, as shown in Fig. 4.15. A Hamming window with a window length of 512 samples and a sampling frequency of 30.72 MHz were used.

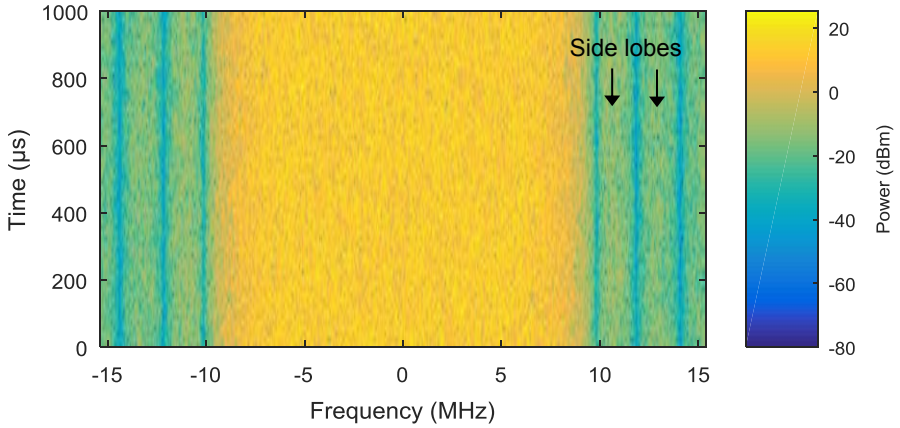

Figure 4.15: Spectrogram of the filtered QPSK signal (1 ms)

The bandwidth of the filtered QPSK signal was constant within the period of the spectrogram. Contrary to the LTE and SC-FDMA signals, there were no periodic bursts. Vertical bands were seen on each side of the spectrogram, corresponding to the side lobes in the spectral leakage of the RRC filter.

The power spectrum of the filtered QPSK signal was measured using a periodogram with a window length of 1024 samples. The complex magnitude of the samples used for spectrum analysis is plotted in Fig. 4.16. The complex magnitude of the filtered QPSK signal showed significant variations that were not present in unfiltered QPSK signal. It can be concluded that while a continuous waveform cannot emulate a QPSK signal with amplitude variations due to filtering of the signal. The samples had peak amplitude of 5.6 V, for a PAPR of 4.96 dB.

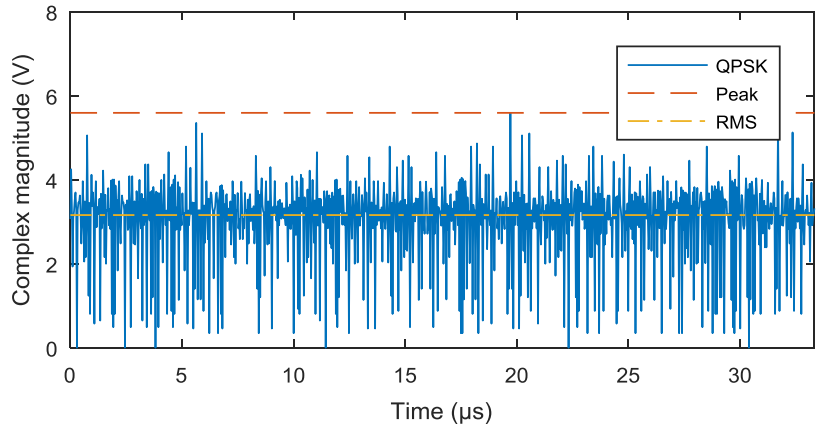

Figure 4.16: Complex magnitude of 1024 QPSK samples

As for LTE and SC-FDMA, a rectangular window function was used for the power spectrum estimate with a RBW of 30 kHz. The frequency response of the RRC filter was estimated using Matlab's freqz function: the spectrum of the QPSK signal matched the frequency response of the RRC filter. The power spectrum of the filtered QPSK signal was found to be mostly lower than the SEM limits, as shown in Fig. 4.17. It was estimated that the probability of the filtered QPSK signal exceeding the SEM limits was negligible.

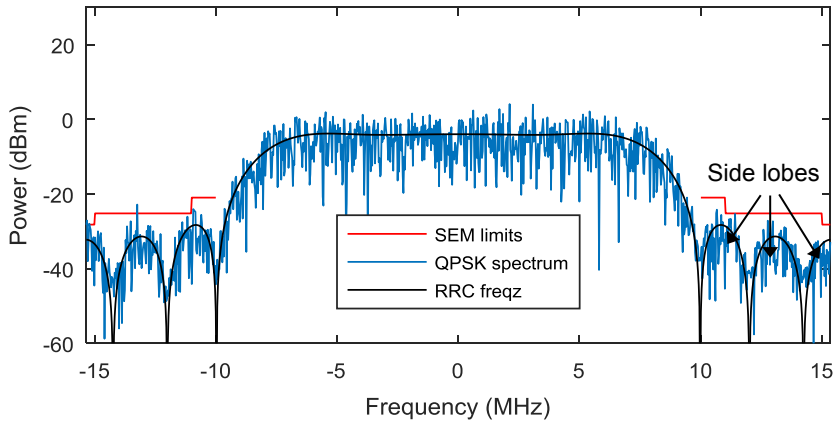

Figure 4.17: Spectrum of QPSK, RRC freqz and SEM limits, RBW of 30 kHz

Another periodogram was used to estimate the power spectrum of filtered QPSK with a RBW of 1 MHz. The periodogram of the QPSK signal using a Hann window with a length of 47 samples was found to be within the SEM limits adjusted for a RBW of 1 MHz, as shown in Fig. 4.18.

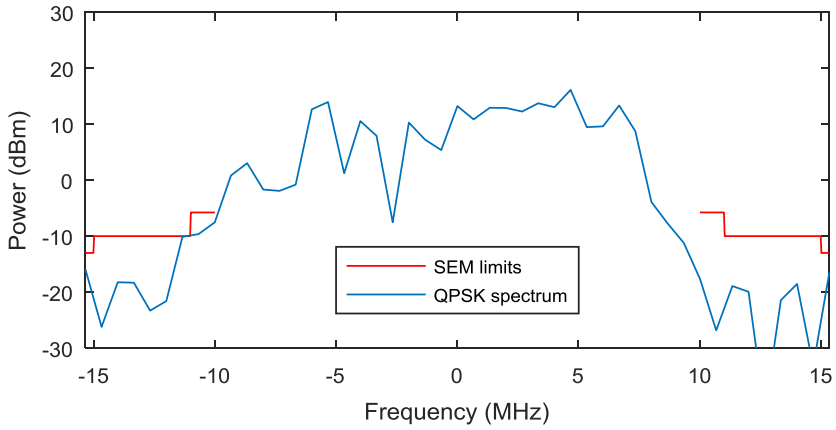

Figure 4.18: Spectrum of QPSK and SEM limits, RBW of 1 MHz

By choosing the span, the upsampling factor, and the roll-off factor of the RRC filter, it was possible to attenuate the spectrum of the filtered QPSK signal to within the SEM limits. The power spectrum of the QPSK signal can be considered similar to the spectrum of the LTE and SC-FDMA signals, except for the lack of out-of-band bursts that were associated to the transitions between symbols.

4.4.3 PAPR of the filtered QPSK signals

The PAPR and CCDF probabilities of the filtered QPSK signal were measured, and compared to the PAPR and the CCDF probabilities of the LTE signals, as shown in Fig 4.19. The PAPR of the QPSK signal was found to be significantly lower than the PAPR of the LTE signals: a test waveform with QPSK modulation could be used as a lower bound for the PAPR of the LTE waveforms.

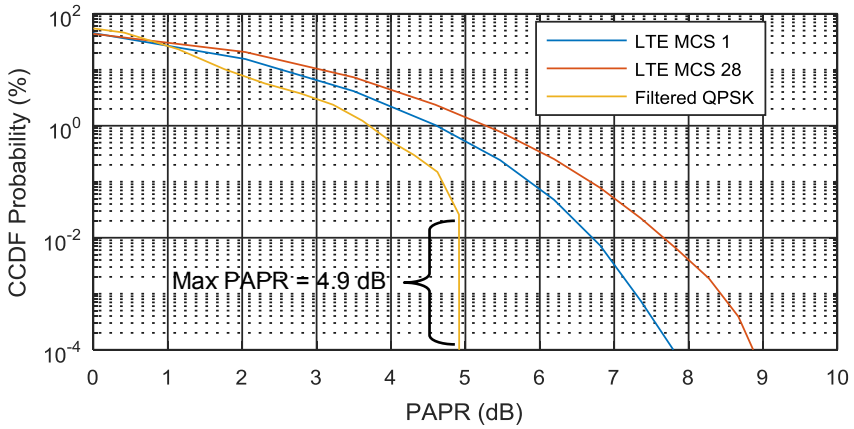

Figure 4.19: PAPR of LTE and filtered QPSK signals

For the range of CCDF probabilities from 0.0025 % to 0.0001 %, the PAPR of the QPSK signal was constant with a value of 4.9 dB. This can be explained by the fact that a limited number of QPSK symbols can fit in the span of the RRC filter. After a specific number of samples, all the possible combinations of QPSK symbols in the filter span have been generated, and the peak magnitude of the signal stop increasing, yielding a constant PAPR value. Characteristics of the RRC filter such as the upsampling factor and the filter span can affect the CCDF probability value upon which the PAPR of a QPSK signal becomes constant.

4.5 Filtered noise waveform design

4.5.1 Noise signals with a Gaussian probability distribution

Matlab's randn function was used to generate a random noise signal with a Gaussian (normal) probability distribution, as shown on the histogram in Fig. 4.20. The variance of the random noise signal was chosen arbitrarily, and the signals were normalized to a power of 23 dBm after filtering.

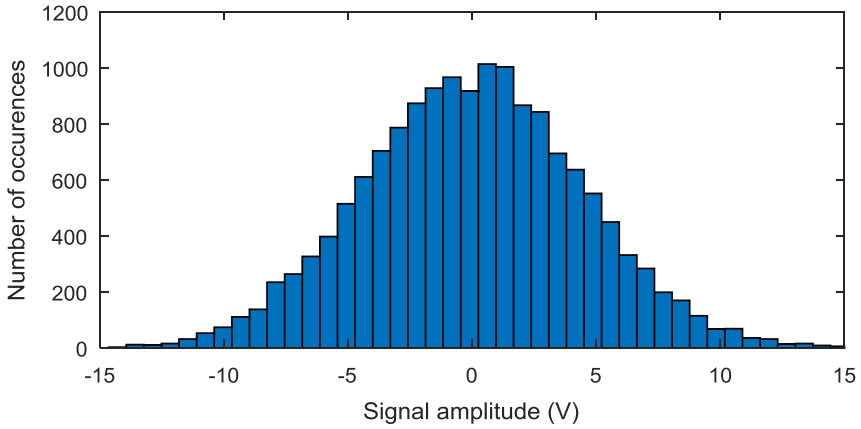

Figure 4.20: Histogram of the Gaussian probability distribution

The Gaussian noise signal was filtered with the same RRC filter that had been used for QPSK signals. The amplitude of 1024 samples within the filtered Gaussian noise signal was plotted, as shown on Fig. 4.21.

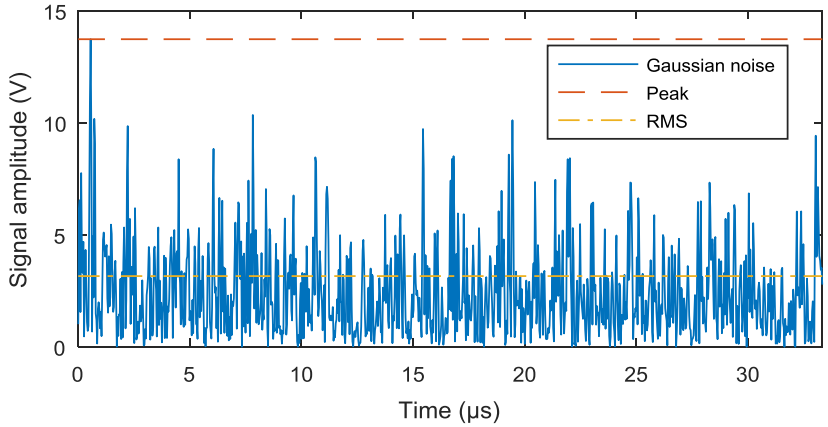

Figure 4.21: Amplitude of 1024 Gaussian noise samples

The amplitude of the Gaussian noise signal had a much higher variations than the LTE, the SC-FDMA, and the QPSK signals. When normalized for RMS amplitude of 3.16 V, the Gaussian noise samples had peak amplitude of 13.7 V, for a PAPR of 12.8 dB. Further PAPR analysis will be presented in Section 4.5.3.

4.5.2 Noise signals with a uniform probability distribution

Matlab's rand function was used to generate a random noise signal with a uniform probability distribution, as shown on the histogram in Fig. 4.22.

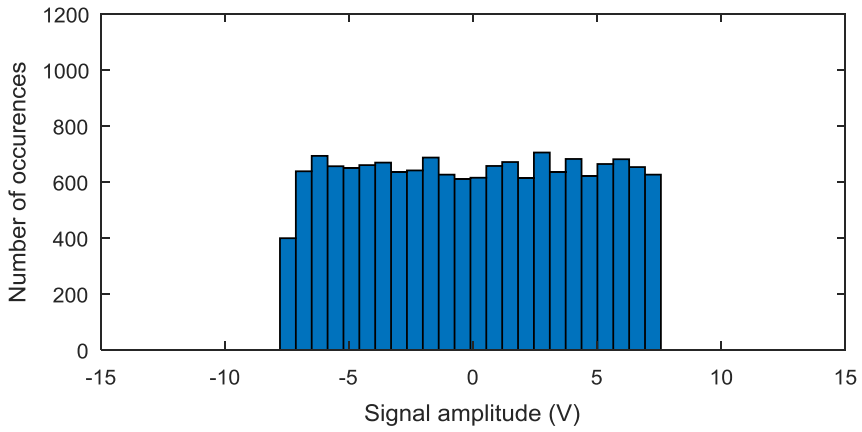

Figure 4.22: Histogram of the uniform probability distribution

The uniform noise was filtered with the same RRC filter. The magnitude of 1024 samples within the uniform noise signal was plotted, as shown on Fig. 4.23.

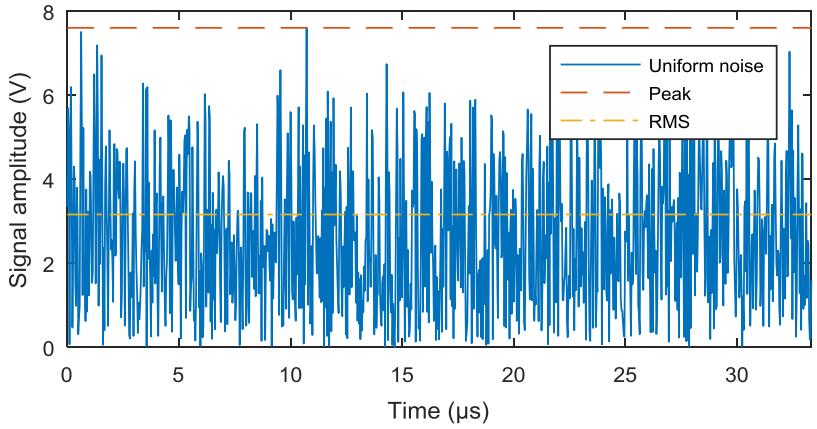

Figure 4.23: Amplitude of 1024 uniform noise samples

The amplitude of the Gaussian noise signal had variations that were much akin to those observed in LTE, the SC-FDMA, and the QPSK signals. The uniform noise samples had peak amplitude of 7.6 V, for a PAPR of 7.6 dB.

4.5.3 PAPR of the noise signals

Matlab's CCDF system object was used to measure the PAPR of uniform and Gaussian noise signals. The PAPR of the uniform noise and of the Gaussian noise were compared to the PAPR of LTE signals, as shown in Fig 4.24.

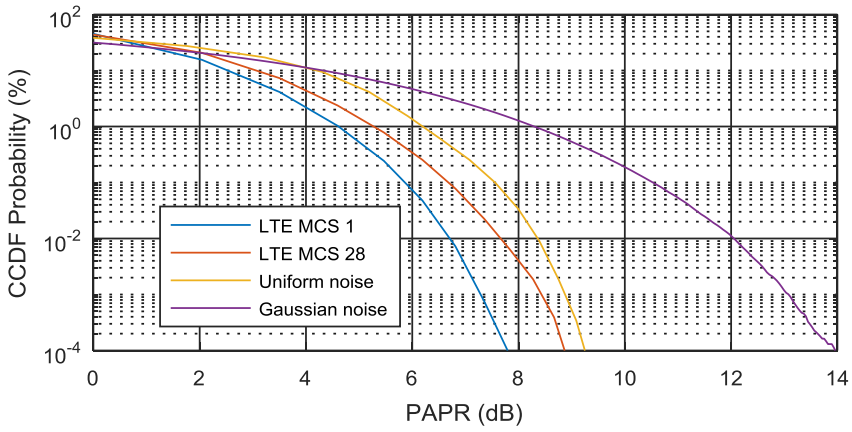

Figure 4.24: PAPR of LTE, uniform and Gaussian noise signals

The PAPR of the Gaussian noise signal was significantly higher than the PAPR of the uniform noise signal: for a CCDF probability of 0.0001%, the Gaussian noise had a PAPR of 14 dB, whereas the uniform noise had a PAPR of 9.2 dB. As vector signal generators and amplifiers have a limited power output, the peak power of test waveforms must be limited. The PAPR of the Gaussian noise signal is higher than what is necessary to be representative of the LTE signals. Yet, the PAPR of the uniform noise signal have been slightly higher than the PAPR of LTE. The uniform probability distribution was therefore chosen for the design of noise signals, to be used as a higher bound for the PAPR of the LTE signals.

4.5.4 Spectrum of the noise signals

The spectrogram of the filtered uniform noise signal is shown in Fig. 4.25. A Hann window length of 512 samples and a sampling frequency of 30.72 MHz were used.

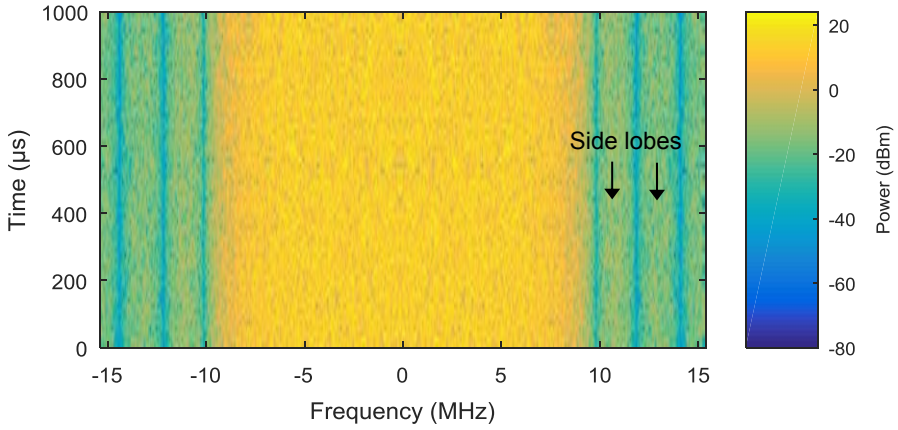

Figure 4.25: Spectrogram of the filtered noise signal (1 ms)

The spectrogram of the filtered noise signal was found to be almost identical to the spectrogram of the filtered QPSK signal. The spectrum of the filtered noise was compared to the SEM limits with a RBW of 30 kHz, as shown in Fig. 4.26.

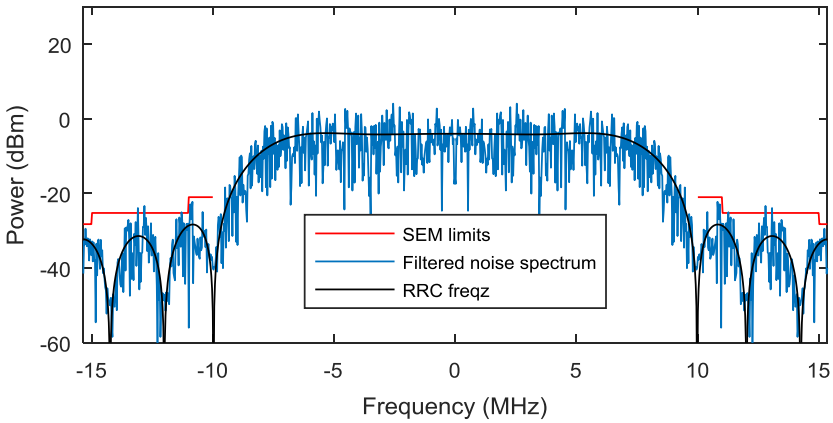

Figure 4.26: Spectrum of filtered noise and SEM limits, RBW of 30 kHz

The periodogram of the filtered noise using a rectangular window with a window length of 1024 samples was found to be slightly exceeding the SEM limits adjusted for a RBW of 30 kHz. However, the exceedance power was negligible. Again, the spectrum of the filtered noise signal was found to be almost identical to the filtered QPSK signal. Similar to the QPSK signal, the frequency response of the noise signal was determined by the RRC filter. The parameters of the RRC filter can be chosen to attenuate of the noise signal in the out-of-band frequencies.

The spectrum of the filtered noise was also compared to the SEM limits with a RBW of 1 MHz, as shown in Fig. 4.27. Similar to the spectrum analysis of LTE, SC-FDMA and QPSK signals; a periodogram function with a Hann window, and a window length of 47 samples was used.

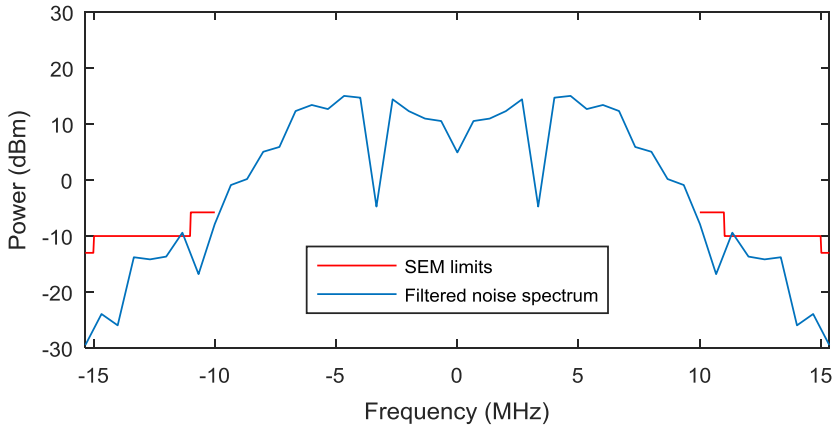

Figure 4.27: Spectrum of filtered noise and SEM limits, RBW of 1 MHz

The power spectrum of the filtered noise signal was found to be lower than the SEM limits adjusted for a RBW of 1 MHz. The spectrum of the filtered noise signal was symmetrical, because there is no imaginary part to the signal.

4.6 Pulse modulated waveform design

As described in Section 2.4.2, a study performed by NASA found that a pulse's rise time has an effect on the susceptibility [9]. Rapid changes of the transmitted power in the signal bursts create a rising edge when the transmitter is turned on; and a falling edge when the transmitter is turned off. In this section, the parameters of a pulse modulated waveform will be selected to emulate the SRS blanking in LTE. The length of the rising and falling edges will be chosen so that their frequency responses conform to the SEM limits in the LTE standard.

4.6.1 SystemVue model for the pulse modulated signals

Keysight's SystemVue software was used to generate a pulse modulated signal. The design schematic of the signal generator is shown in Fig. 4.28. A pulse generator, with a low voltage level of 0 volts, a high voltage level of 0.398 V, a period of 5 ms, and a pulse width of 4.929 ms, was connected to the input of a complex to envelope converter. The resulting signal had a power of 23 dBm, and a blanking period of 71 µs. The rising and falling edges had a length of 64 samples, to conform to 10 MHz SEM limits. A signal downloader for Keysight's VSG M9381A, and a data sink with output to a CSV file, were used to record the signal.

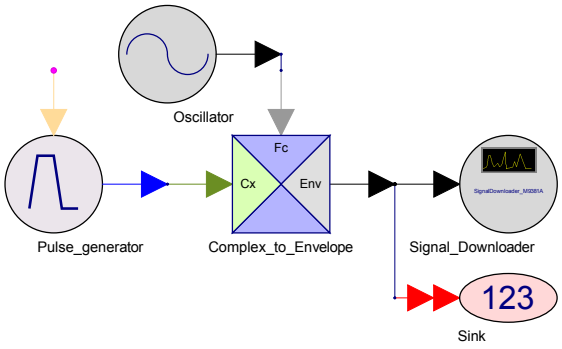

Figure 4.28: Design schematic of the pulse modulated signal generator

4.6.2 Trapezoidal pulse model

The rapid change of transmitted power in a pulse modulated signal creates a rising edge when the transmitter is turned on; and a falling edge when the transmitter is turned off. A trapezoidal pulse signal can be modeled with amplitude A, period T, pulse rise time τ_r, pulse fall time τ_f, and pulse width τ, as shown in Fig. 4.29 [1].

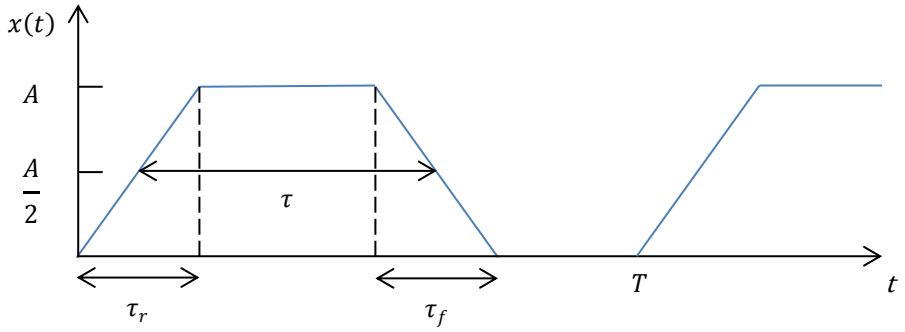

Figure 4.29: Trapezoidal pulse signal model [1]

4.6.3 Fourier series analysis

With a Fourier series analysis of the trapezoidal pulse, it can be shown that when the rise and fall time decreases, the spectrum of the signal widens. When the rise and fall times are equal $(\tau_r = \tau_f)$, the envelope of the one-sided spectrum (positive frequencies) of the signal can be expressed in (4.2) [1].

$$\text{Envelope} = 2A\frac{\tau}{T}\left|\frac{\sin(\pi\tau f)}{\pi\tau f}\right|\left|\frac{\sin(\pi\tau_r f)}{\pi\tau_r f}\right| \tag{4.2}$$

When the rise time is much smaller than the pulse width $(\tau \gg \tau_f)$, and the width is almost equal to the period $(\tau \approx T)$, the envelope of the one-sided spectrum (positive frequencies) can be reduced to the normalized sinc function in (4.3).

$$\text{Envelope} = 2A\left|\frac{\sin(\pi\tau_r f)}{\pi\tau_r f}\right| = 2A|\text{sinc}(\tau_r f)| \tag{4.3}$$

4.6.4 Spectrum of the pulse modulated signals

The spectrogram of a pulse modulated signal with a 71 µs blanking period was plotted and a ruse time of 0.8 µs, as shown in Fig. 4.30. A Hann window of 512 samples and a sampling frequency of 30.72 MHz were used.

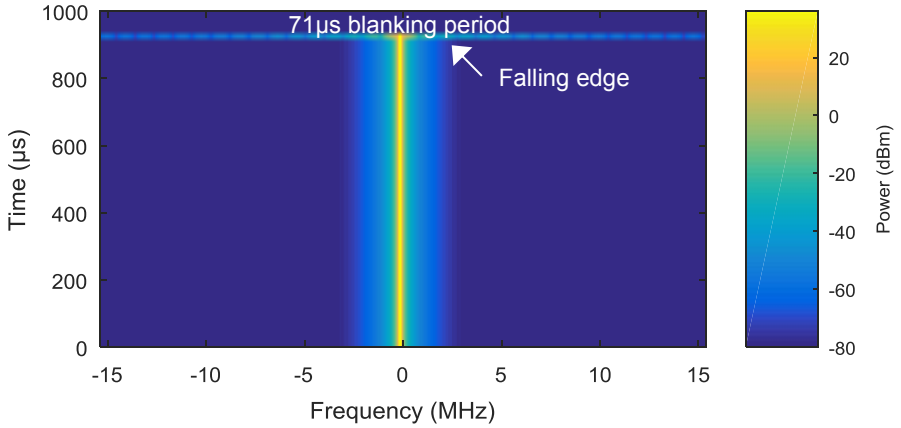

Figure 4.30: Spectrogram of the pulse modulated signal (1 ms)

Out-of-band bursts were seen on each side of the pulse modulated signal, corresponds to the falling edge. The bursts showed some signs of attenuations that were similar to the periodic bursts in Fig. 4.3. The short dashes represent the side lobes of the sinc pattern that resulted from the FFT in the spectrogram.

To compare the power spectrum of the pulse modulate signal to the SEM limits with a RBW of 30 kHz, a rectangular window with a window length of 1024 samples was used. The samples had rising edge with a rise time of 0.8 µs. The power spectrum of the pulse signal was compared to the envelope of the trapezoidal pulse, corresponding to a sinc function, and to the SEM limits with a RBW of 30 kHz, as shown in Fig. 4.31. The spectrum of the pulse signal with a rise time of 0.8 µs was found to be lower than the SEM limits for a 20 MHz channel bandwidth. The spectrum of the pulse signal was also found to be

matching the amplitude of the sinc function. A power of 23 dBm was measured at the DC frequency, corresponding to the constant signal with amplitude of 3.16 V.

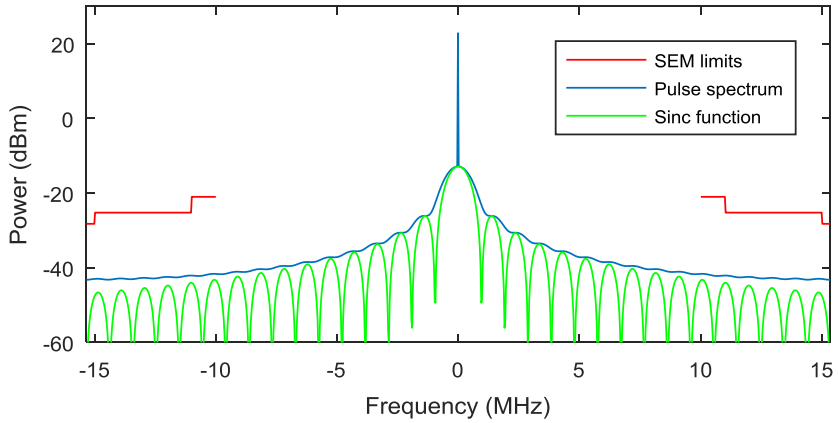

Figure 4.31: Spectrum of pulse, sinc function and SEM limits, RBW of 30 kHz

The power spectrum estimate of the pulse modulated signal using a rectangular window and a window length of 31 samples was found to be matching the SEM limits, and the the sinc function for a RBW of 1 MHz, as shown in Fig. 4.32.

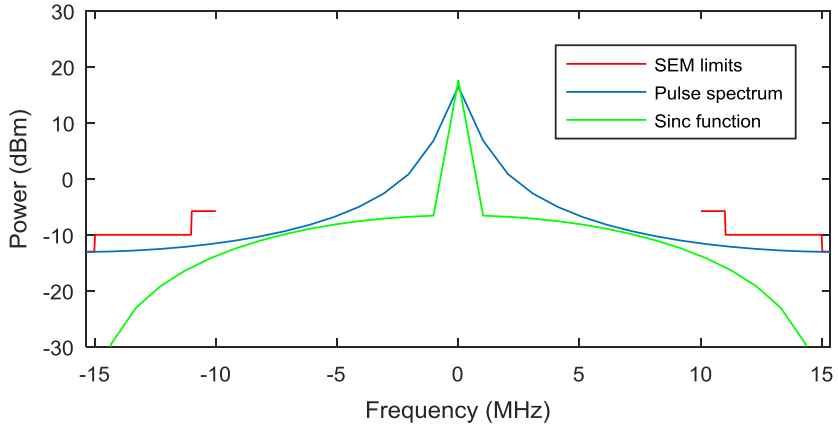

Figure 4.32: Spectrum of pulse, sinc function and SEM limits, RBW of 1 MHz

4.7 Choice of test waveforms parameters

Five frequency bandwidths were chosen for the design of test waveforms, to match five of the six channel bandwidths available for LTE: 1.4, 3, 5, 10, and 20 MHz. LTE's 15 MHz channel bandwidth was excluded to simplify the design process. The five channel bandwidths and the five signal modulations resulted in 25 test waveforms, as listed in Table 4.2.

Table 4.2: List of test waveforms bandwidths and modulation

Modulation	Channel bandwidth				
	1.4 MHz	3 MHz	5 MHz	10 MHz	20 MHz
LTE	1a	1b	1c	1d	1e
SC-FDMA	2a	2b	2c	2d	2e
QPSK	3a	3b	3c	3d	3e
Noise	4a	4b	4c	4d	4e
Pulse	5a	5b	5c	5d	5e

The sampling frequencies and oversampling ratios that were used in the design of LTE waveforms are listed in Table 4.3. A sampling frequency of 15.36 MHz and an oversampling ratio of 8 were used for LTE with a 1.4 MHz channel bandwidth. A sampling frequency of 30.72 MHz and oversampling ratios of 8, 4, 2, and 1 were used for LTE with 3, 5, 10 and 20 MHz, respectively.

Table 4.3: Sampling frequencies and LTE oversampling ratios

LTE waveform number	1a	1b	1c	1d	1e
Channel bandwidth [MHz]	1.4	3	5	10	20
Sampling frequency [MHz]	15.36	30.72	30.72	30.72	30.72
Oversampling ratio	8	8	4	2	1

The numbers of subcarriers for SC-FDMA waveforms were chosen to match the channel bandwidths, as listed in Table 4.4. A FFT length of 2048 samples and a sampling frequency of 30.72 MHz were used for all SC-FDMA waveforms.

Table 4.4: Maximum number of subcarriers for SC-FDMA

SC-FDMA waveform number	2a	2b	2c	2d	2e
Channel bandwidth [MHz]	1.4	3	5	10	20
Number of subcarriers	72	180	300	600	1200

The upsampling factors in the RRC filters were chosen to match the channel bandwidths, as listed in Table 4.5. A span of 6 samples, a roll-off factor of 0.22 and a sampling frequency of 30.72 MHz were used for all filtered waveforms.

Table 4.5: RRC upsampling factors

QPSK/Noise waveform number	3a/4a	3b/4b	3c/4c	3d/4d	3e/4e
Channel bandwidth [MHz]	1.4	3	5	10	20
RRC filter upsampling factor	32	16	8	4	2

The rise times of the pulse modulation were chosen to match the channel bandwidths, as listed in Table 4.6. A pulse repetition interval of 5 ms and a sampling frequency of 30.72 MHz were used for all pulse modulated waveforms.

Table 4.6: Rise time and measurement bandwidth of ramp function

Pulse modulated waveform number	5a	5b	5c	5d	5e
Channel bandwidth [MHz]	1.4	3	5	10	20
Rise time [µs]	12.8	6.4	3.2	1.6	0.8

4.8 PAPR analysis and comparison

In Section 4.1.3, two LTE waveforms were generated: one with a MCS index of 1 (QPSK), and another with a MCS index of 28 (64-QAM). The PAPR CCDFs of both LTE waveforms were compared to those of the other waveforms with a 20 MHz channel bandwidth. In this section, the effect of the variation of channel bandwidths introduced in Section 4.7 will be evaluated for the LTE, SC-FDMA, filtered QPSK and filtered noise waveforms.

4.8.1 MCS index 1 and QPSK symbol mapping

The PAPR was computed for 200 LTE slots with a MCS index of 1 (QPSK), and channel bandwidths of 1.4, 3, 5, 10, and 20 MHz. For each of the channel bandwidths, the mean PAPR value was calculated. The same PAPR analysis process was repeated for SC-FDMA with QPSK symbol mapping, filtered noise, and filtered QPSK. The mean PAPR values were plotted using Matlab's semilogx function, as shown in Fig. 4.33.

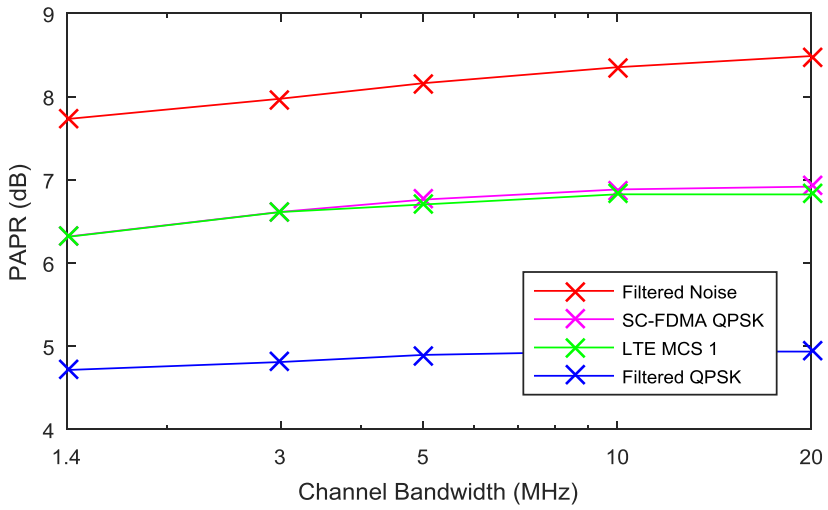

Figure 4.33: Mean signal PAPR and Bandwidth Analysis (MCS1)

Comparison of the mean PAPR values showed that the filtered noise waveforms had the highest mean PAPR, and that the filtered QPSK waveforms had the lowest mean PAPR. Similar to the PAPR CCDF analysis, LTE and SC-FDMA waveforms had similar mean PAPR values. It was observed that the waveforms with the lowest bandwidths had lower PAPR values than the waveforms with the highest bandwidths.

4.8.2 MCS index 28 and 64-QAM symbol mapping

The PAPR analysis was repeated for LTE with a MCS index of 28 and SC-FDMA with 64-QAM symbol mapping, as shown in Fig. 4.34. As found in Section 4.2.3 and 4.3.3, the PAPR of LTE with a MCS index of 1 and SC-FDMA with QPSK symbol mapping are lower than the PAPR of LTE with a MCS index of 28 and SC-FDMA with 64-QAM symbol mapping.

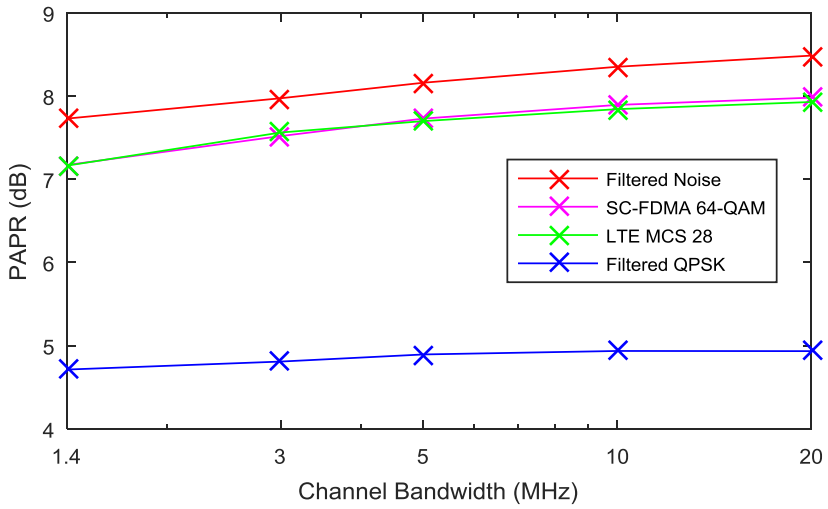

Figure 4.34: Mean signal PAPR and Bandwidth Analysis (MCS28)

4.9 Summary

Five test waveforms were created using a parameter reduction process: LTE, SC-FDMA, QPSK, uniform noise, and pulse modulated. Each waveform was designed for five channel bandwidths: 1.4, 3, 5, 10, and 20 MHz, for a total of 25 test waveforms. The SEM limits were used to set certain parameters of the waveforms such that their frequency content was similar to each other.

The PAPR of the simulated LTE, SC-FDMA, QPSK, and noise waveforms were measured. LTE and SC-FDMA waveforms had similar PAPR values. The PAPR of QPSK waveforms was significantly lower than the PAPR of the noise waveforms. The QPSK and noise waveforms formed lower and higher bounds for the PAPR of the LTE and the SC-FDMA waveforms, respectively.

The parameters of the waveforms were carefully selected to ensure a fair comparison of radiated susceptibility test results. RRC filters with similar characteristics were used to limit the bandwidth of QPSK and noise waveforms. The pulse modulated waveform's repetition interval and duty factor emulated the SRS blanking in LTE. The lengths of the rising and falling edges were chosen to match the SEM limits. Finally, the MCS index for LTE and the symbol mapping for SC-FDMA were chosen to limit the PAPR of those waveforms.

5 Radiated susceptibility testing

In the previous chapter, a parameter reduction process was used to design 25 test waveforms that were estimated to be representative of the LTE communication standard. In this chapter, radiated susceptibility testing will be undertaken to compare these susceptibility results using the different waveforms. The choice of a victim system will be explained, followed by the description of the radiated test setup and the analysis of the victim's response to the different test waveforms.

5.1 Choice of victim system

While recording the LTE signals in a laboratory environment, it was discovered that interference was induced by mobile phones radiating LTE emissions in close proximity to audio devices. It was suspected that the radiated signal was coupled to the cables or to the internal components of the devices, which is a form of back-door interference. For the purpose of this thesis, a victim audio system that would typically be found in an aircraft cockpit environment was chosen.

The PS engineering PM1000II intercom system was chosen as a victim system [14]. The PM1000II is panel mounted, with volume and squelch controls for the pilot and the copilot, as shown in Fig. 5.1. The PM1000II is approved by the FAA for use in aircraft, and is certified according to the RTCA DO-160B standard. The cable harness, model 12112, was used to provide the power and to provide the input and output jacks to the PM1000II.

Figure 5.1: PS Engineering PM1000II intercom system

It was suspected that the PM1000II had an internal filter to attenuate the frequencies that are not within the audible range. The frequency response of the filter was measured by varying an input signal and measuring the output signal. A signal with peak-to-peak amplitude of 60 mV was applied to the auxiliary input, while the volume amplifier controls were set to the maximum. The pilot's headphone output was measured using an oscilloscope. The peak-to-peak amplitude of the output signal was recorded, and the frequency response was plotted using Matlab's semilogx function, as shown in Fig. 5.2.

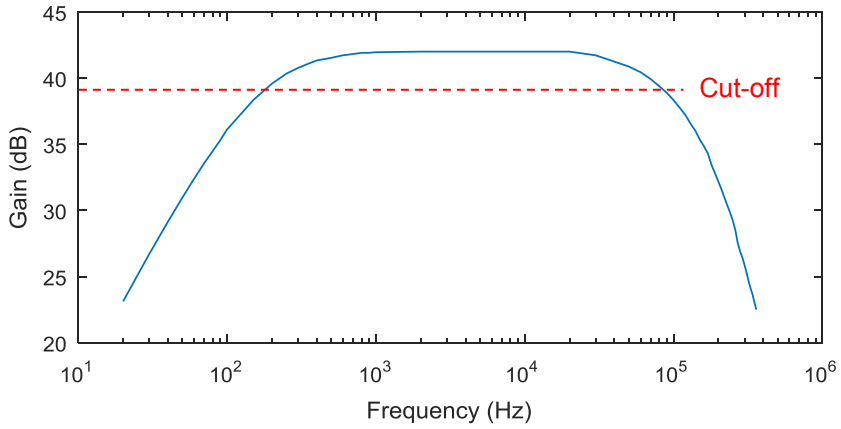

Figure 5.2: Frequency response of the PM1000II intercom system

The frequency response of the PM1000II was similar to that of a passband filter. The maximum peak-to-peak amplitude of the output signal was recorded at 7.56 V, corresponding to a gain of 42 dB. The cut-off frequencies were evaluated for a gain of 39 dB, or 3 dB lower than the gain in the passband. A lower cut-off frequency was found at 180 Hz, and a higher cut-off frequency was found at 90 kHz, which is beyond the 20 kHz audible limit.

5.2 Radiated susceptibility testing setup

Once the PM1000II was chosen as a victim system for radiated susceptibility testing, it was necessary to construct a setup that would permit the radiated susceptibility testing for the various test waveforms. The setup was made of four elements, as shown in Fig. 5.3: a vector signal generator (VSG), an antenna, a device under test (DUT), and an oscilloscope. Keysight's M9381A vector signal generator was used to transmit the test waveforms [15], whereas L-Com's HG908P patch antenna was used to radiate the amplified test waveforms [16]. The DUT was the PM1000II with its cable harness, as described in the previous section. Tektronix's MSO4104 mixed signal oscilloscope was used to record the interference signals from the DUT output [17].

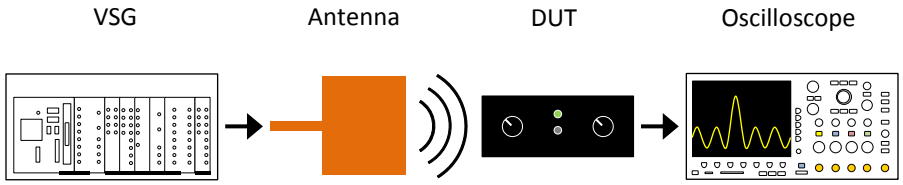

Figure 5.3: Radiated susceptibility testing setup

5.2.1 Vector signal generator setup

The VSG was installed outside an anechoic chamber. As described in Section 4.7, a sample rate of 30.72 MHz was used for all waveforms, except for the LTE waveform with a bandwidth of 1.4 MHz (sample rate of 15.36 MHz). The source output of the vector signal generator was set to a RMS power of -9 dBm for all waveforms. An amplifier provided a gain of 25 dB, for a total transmitted power of 16 dBm. All waveforms used the same transmitted power.

5.2.2 Antenna and DUT setup

The antenna and the DUT were installed in an anechoic chamber, as shown in Fig. 5.4. The DUT was positioned in close proximity to the antenna. It was found that the position that yielded the highest coupling was when the connector of the cable harness was aligned on the center of the antenna. The cable harness of the PM1000II and the cable of the antenna were kept in the same position to ensure that the coupling did not vary during radiated susceptibility testing. The enclosure of the PM1000II was not grounded. The volume amplifier controls were set to the maximum, and the squelch controls were set to the minimum in order to produce the highest level of interference.

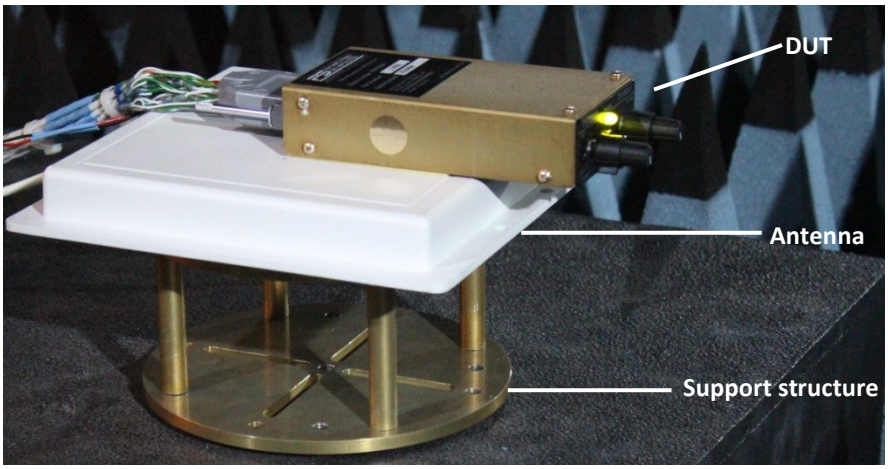

Figure 5.4: Antenna and DUT setup in the anechoic chamber

5.2.3 Oscilloscope setup

The oscilloscope was installed outside the anechoic chamber. The cable for the pilot headphone output of the PM1000II was connected to the Tektronix MSO 4104 oscilloscope. A sampling frequency of 5 million samples per second and a recording of one million samples were used, for a recording length of 200 ms. A DC coupling and an impedance of 50 ohms were used.

5.3 Interference induced by the test waveforms

Using the setup that was described in the previous section, the interference signals were recorded, and converted to a Matlab database for analysis. In this section, the analysis results and a comparison of the interference signals will be presented.

5.3.1 LTE waveforms

The interference signal induced by the LTE waveform with a 1.4 MHz bandwidth is plotted in Fig. 5.5. A delay was used to center the blanking period on the graph.

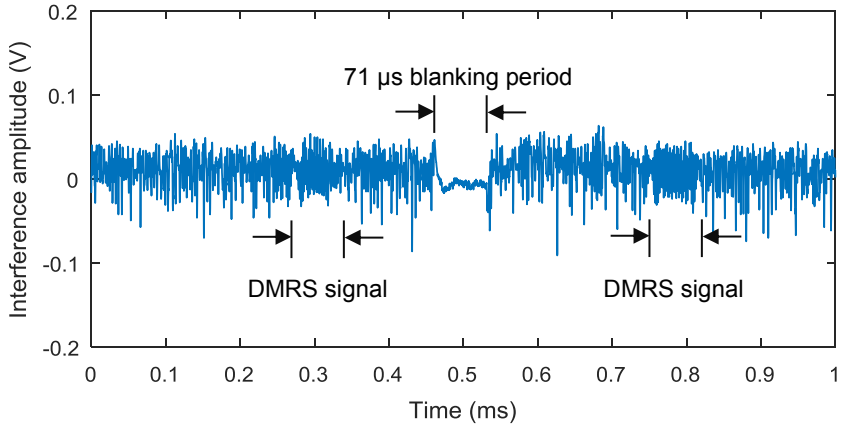

Figure 5.5: Interference signal induced by the LTE waveform, 1.4 MHz BW

The interference signal had a significant reduction in its amplitude for a duration of 71 µs, corresponding to the SRS blanking period. The effect of the DMRS signals was also observed, corresponding to two periods of relatively constant amplitude. The amplitude of the interference signals varied significantly in the remaining periods of the subframe.

To determine the effect of an increase in the signal bandwidth, the interference signal induced by the LTE waveform with a bandwidth of 20 MHz was also plotted for a period of 1 ms, as shown in Fig. 5.6.

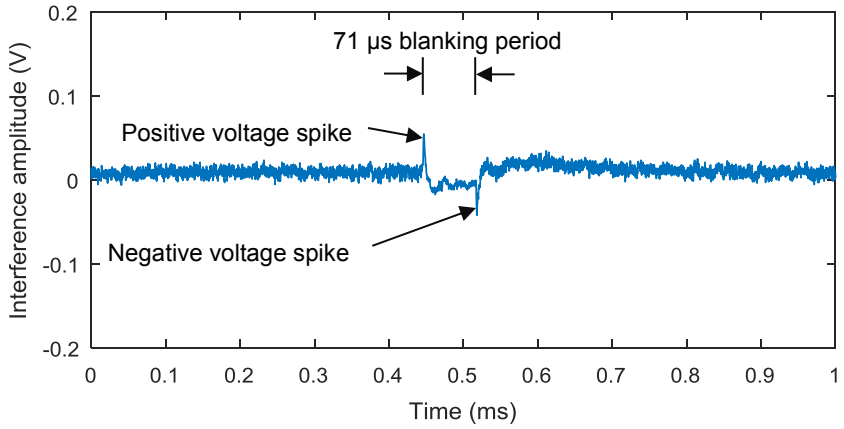

Figure 5.6: Interference signal induced by the LTE waveform, 20 MHz BW

The amplitude of the interference induced by the LTE waveform with a bandwidth of 20 MHz was found to be significantly smaller than that for 1.4 MHz. It can be deducted that the DUT filtered the spectrum that was higher than the cut-off frequency of 90 kHz. A positive voltage spike was associated with the falling edge of the interfering signal, and a negative voltage spike with its rising edge.

Matlab's normfit function was used to compute the mean µ and the standard deviation σ with a sample size *n* of 20 for each waveform. The computed values for a carrier frequency of 700 MHz are shown in Table 5.1.

Table 5.1: Interference induced by LTE waveforms

Waveform	Channel	RMS Power		Peak Power	
Number	Bandwidth	µ (dBm)	σ (dB)	µ (dBm)	σ (dB)
1a	1.4 MHz	-20.43	0.02	-5.88	0.25
1b	3 MHz	-24.22	0.03	-11.58	0.47
1c	5 MHz	-25.53	0.02	-12.71	0.38
1d	10 MHz	-26.23	0.05	-12.82	0.33
1e	20 MHz	-26.45	0.05	-12.53	0.38

5.3.2 SC-FDMA waveforms

Similar to the interference signals induced by the LTE waveforms, the amplitude of the interference signals caused by the SC-FDMA waveforms varied significantly. There was no repeating pattern in the interference signal, due to the lack of SRS blanking period or DMRS. Using the same process as for LTE, the mean RMS and peak power of the interference signals produced by the SC-FDMA waveforms were calculated. RMS and peak power of the interference induced by SC-FDMA waveforms with a carrier frequency of 700 MHz are shown in Table 5.2.

Table 5.2: Interference induced by SC-FDMA waveforms

Waveform	Channel	RMS Power		Peak Power	
Number	Bandwidth	μ (dBm)	σ (dB)	μ (dBm)	σ (dB)
2a	1.4 MHz	-21.63	0.02	-6.73	0.34
2b	3 MHz	-24.63	0.04	-13.57	0.46
2c	5 MHz	-25.35	0.04	-15.15	0.31
2d	10 MHz	-26.04	0.04	-16.89	0.47
2e	20 MHz	-26.19	0.03	-17.89	0.37

The RMS power of the interference signals induced by the SC-FDMA was similar to those of LTE. However, the peak power was significantly lower, especially for the larger channel bandwidths. It can be deduced that the blanking periods have a significant effect on peak power of the interference signals, but not on the RMS power. It can also be deduced that the DMRS signals do not have a significant effect on neither the RMS nor the peak power of the interfering signals. As for LTE, the SC-FDMA waveforms with a small channel bandwidth yielded higher RMS interference than those with large channel bandwidths.

5.3.3 Filtered QPSK waveforms

The computed values for the interference signals induced by filtered QPSK waveforms with a carrier frequency of 700 MHz are listed in Table 5.3.

Table 5.3: Interference induced by QPSK waveforms

Waveform	Channel	RMS Power		Peak Power	
Number	Bandwidth	μ (dBm)	σ (dB)	μ (dBm)	σ (dB)
3a	1.4 MHz	-21.73	0.02	-11.04	0.24
3b	3 MHz	-23.38	0.03	-13.24	0.22
3c	5 MHz	-24.67	0.04	-14.37	0.34
3d	10 MHz	-25.55	0.03	-16.11	0.28
3e	20 MHz	-26.15	0.03	-17.77	0.41

The RMS power of the interference induced by the filtered QPSK waveforms was similar to that of LTE and SC-FDMA. The peak power of the interference induced by the QPSK waveforms was similar to the peak power of the interference caused by SC-FDMA, and lower than the peak power of the interference caused by LTE. It is suspected that the effect of digital modulation could be less significant than the effect of the discontinuous transmission and the effect of the PAPR.

QPSK is similar to the GMSK used in the GSM communication standard [2]. Therefore, it could be argued that the interference produced by a GSM waveform would be comparable to interference of QPSK waveforms. Due to the fact that the RMS power of the interference signals induced by QPSK is similar to that of LTE's, it could be expected that GSM and LTE signals would cause interference with similar RMS power levels, when testing under the same conditions. However, the interference induced by GSM and LTE could have different peak power values.

5.3.4 Filtered noise waveforms

RMS and peak power values of the interference from filtered noise waveforms with a carrier frequency of 700 MHz are listed in Table 5.4.

Table 5.4: Interference induced by filtered noise waveforms

Waveform	Channel	RMS Power		Peak Power	
Number	Bandwidth	μ (dBm)	σ (dB)	μ (dBm)	σ (dB)
4a	1.4 MHz	-14.05	0.01	-2.32	0.14
4b	3 MHz	-16.08	0.01	-3.97	0.17
4c	5 MHz	-18.65	0.01	-5.97	0.37
4d	10 MHz	-21.23	0.02	-9.12	0.36
4e	20 MHz	-23.38	0.02	-11.95	0.41

The RMS and peak power of the interference signals induced by the filtered noise waveforms were higher the interference caused by LTE, SC-FDMA, and QPSK waveforms. As determined in Section 4.8, the filtered noise waveform had a higher PAPR than the LTE, SC-FDMA, and QPSK waveforms. It could be deduced that the effect of an increase in the PAPR of the test waveforms was more significant than the effect of the discontinuous transmission.

However, because the RMS and peak power of the interference induced by the filtered noise waveforms were significantly higher than those of the interference caused by LTE waveforms, using filtered noise could exceed the testing requirements for radiated susceptibility to the LTE communication standard: the filtered noise waveform could induce interference levels that were not present for the LTE waveforms. Moreover, using filtered noise could be impractical because a higher peak output power is required to transmit waveforms with a higher PAPR.

5.3.5 Pulse modulated waveforms

The interference signal induced by the pulse modulated waveform with a rise time of 12.8 µs is plotted in Fig. 5.7. A delay was used to center the blanking period.

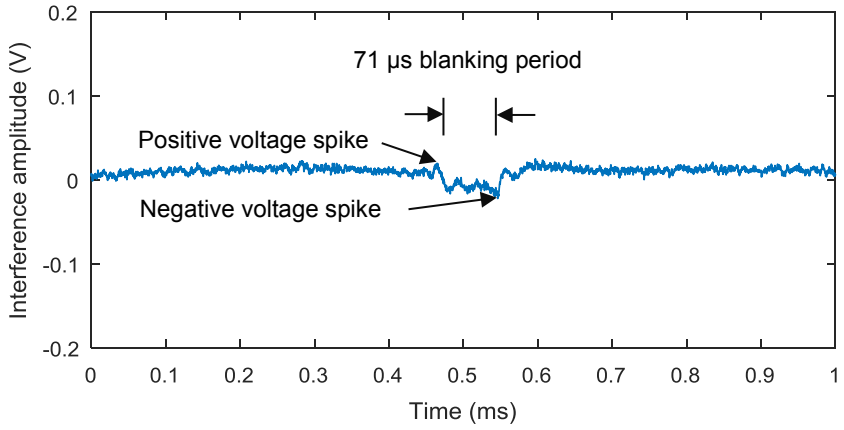

Figure 5.7: Interference signal induced by the pulse waveform, 1.4 MHz BW

The amplitude of the interference signal induced by the pulse modulated waveform was much smaller than the amplitude of the interference signal caused by the other waveforms. The continuous portion of the pulse modulated waveform produced smaller amplitudes than the discontinuous portion. This can be explained by the fact that a continuous wave would typically induce a DC level in the internal components of the DUT, as described in MIL-STD-461 [6]. As measured in Section 5.1, the DUT had a lower cut-off frequency of 180 Hz. Therefore, most of the radiated energy within the continuous portion of the pulse modulated waveform was filtered by the internal components of the DUT.

A blanking period with a length of 71 µs was observed, during which the interference signal had a negative amplitude. The amplitude of the voltage spikes associated with the rising and falling edges were not significantly higher than the rest of the interfering signal.

The interference signal induced by the pulse modulated waveform with a rise time of 0.8 µs is plotted in Fig. 5.8. A delay was used to center the blanking period.

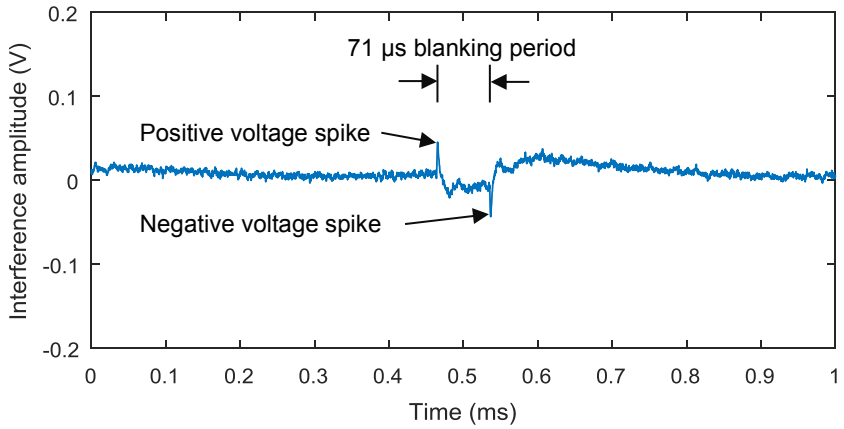

Figure 5.8: Interference signal induced by the pulse waveform, 20 MHz BW

A positive voltage spike was associated with the falling edge of the interfering signal, and a negative voltage spike with its rising edge. When the rising and falling edges had a short rise time, the voltage spikes had significantly higher amplitudes. The computed values for the interference signals induced by pulse modulated waveforms with a carrier frequency of 700 MHz are listed in Table 5.5.

Table 5.5: Interference induced by pulse modulated waveforms

Waveform Number	Channel Bandwidth	Rise time	RMS Power		Peak Power	
			µ (dBm)	σ (dB)	µ (dBm)	σ (dB)
5a	1.4 MHz	12.8 µs	-26.57	0.09	-17.73	1.06
5b	3 MHz	6.4 µs	-26.57	0.09	-16.96	0.55
5c	5 MHz	3.2 µs	-26.55	0.09	-15.19	0.47
5d	10 MHz	1.6 µs	-26.55	0.10	-13.70	0.35
5e	20 MHz	0.8 µs	-26.57	0.07	-13.17	0.42

The peak power of the interference induced by the pulse modulated waveforms was lower than that of the LTE waveforms. In fact, the rise time had been chosen so that the power spectrum of the pulse waveform was always lower than the SEM limits for LTE. As discussed in Section 4.6.4, a rectangular window was used for the spectral analysis of the pulse modulated waveform, which led to the choice of a slower rise time. The use of a Hann window would have led to a faster rise time, and the peak power of the interference induced by the pulse modulated waveforms could have been closer to that of the LTE waveforms.

The peak power of the interference induced by the pulse modulated waveforms was also lower than that of the SC-FDMA waveforms. However, the peak power of the interference produced by pulse modulated waveforms with channel bandwidths of 10 MHz and 20 MHz were significantly higher than the peak power of the interference from QPSK and SC-FDMA waveforms.

Discontinuous transmissions such as the blanking period in pulse modulated waveforms had a significant effect on the peak power of the interference signals. The peak power of the interference caused by LTE with a bandwidth of 1.4 MHz in Fig 5.5 was not related to the discontinuous transmissions, but to the noise-like portion of the LTE waveform that is modulated with SC-FDMA. On the other hand, the peak power of the interference signals induced by the LTE waveform with a bandwidth of 20 MHz in Fig 5.6 was directly related to the rise time of the discontinuous transmissions within the interfering signal.

As the RMS and peak power values of the interference induced by the pulse modulated waveforms were lower than the RMS and peak power values from the LTE waveforms, the validity of using a pulse modulated waveform can be questioned. For the case of the radiated susceptibility test of the DUT at a carrier frequency of 700 MHz, the interference induced by the pulse modulated waveforms were not representative of the interference induced by LTE waveforms.

5.3.6 Comparing the interference power measurements

To compare the RMS and peak power of interference signals induced by the different waveform with a carrier frequency of 700 MHz, two graphs were plotted using Matlab's semilogx function. The RMS power values of the interference signals induced by all waveforms are plotted in Fig. 5.9.

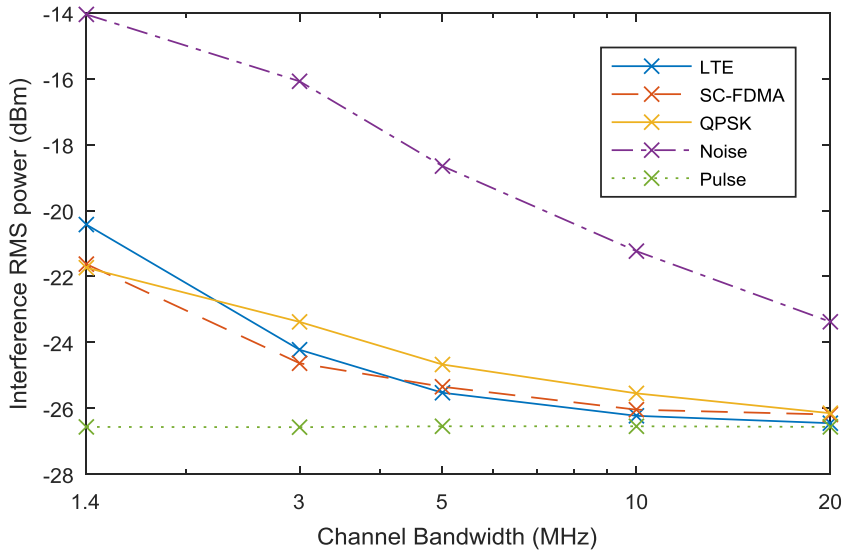

Figure 5.9: RMS power of interference signals, carrier frequency of 700 MHz

Fig. 5.9 shows that the interference induced by the filtered noise waveforms had significantly higher RMS power than of the interference caused by the other waveforms. Moreover, the interference signals induced by the SC-FDMA and the QPSK waveforms had RMS power values that were similar than of the interference signals caused by the LTE signals. The interference signals induced by the pulse modulated signals had the lowest RMS power values. The peak power values of the interference signals induced by all waveforms are plotted in Fig. 5.10.

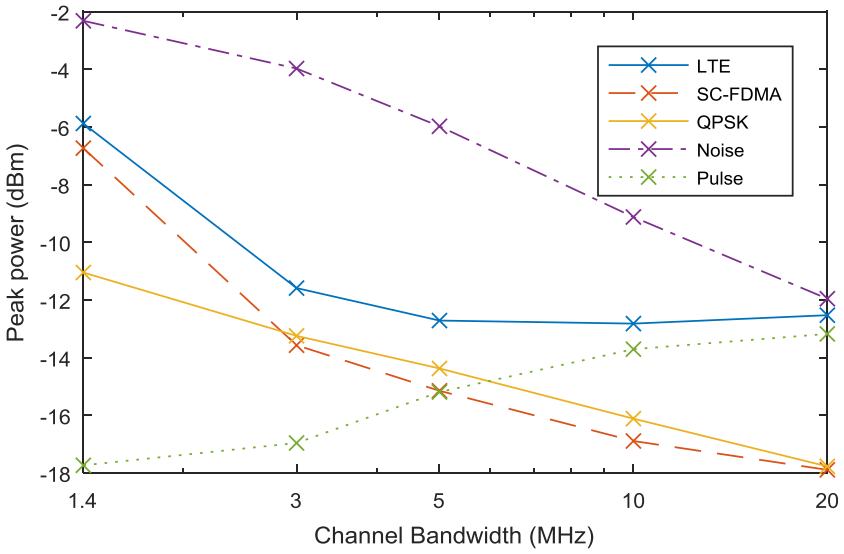

Figure 5.10: Peak power of interference signals, carrier frequency of 700 MHz

The peak power of the interference signals induced by the filtered noise with a channel bandwidth of 20 MHz was similar to that of LTE and pulse modulated waveforms with the same channel bandwidth. For all channel bandwidths, the interference signals induced by the SC-FDMA and QPSK waveforms had a lower peak power than the interference produced by LTE. It was found the pulse modulated waveforms were only able to emulate the discontinuous transmissions in LTE. On the other hand, the SC-FDMA, QPSK, and noise waveforms were only able to emulate the noise-like portions of LTE. The plot of the peak power induced by the pulse modulated waveforms intersects the plot of the peak power induced by the SC-FDMA waveforms at a bandwidth of 5 MHz. When the test waveforms have a bandwidth above a 5 MHz, the discontinuous transmissions induced a higher peak power than the noise-like portion of LTE.

5.3.7 Sweeping carrier frequencies

To observe the effect of a change of the carrier frequency in the test waveforms, carrier frequencies from 700 MHz to 960 MHz were used, corresponding to the lowest band of frequencies allocated for LTE [3]. The frequencies were swept in increments of 10 MHz, resulting in a total of 27 frequency values. The RMS power values of the interference signals induced by waveforms with a channel bandwidth of 1.4 MHz are plotted in Fig. 5.11.

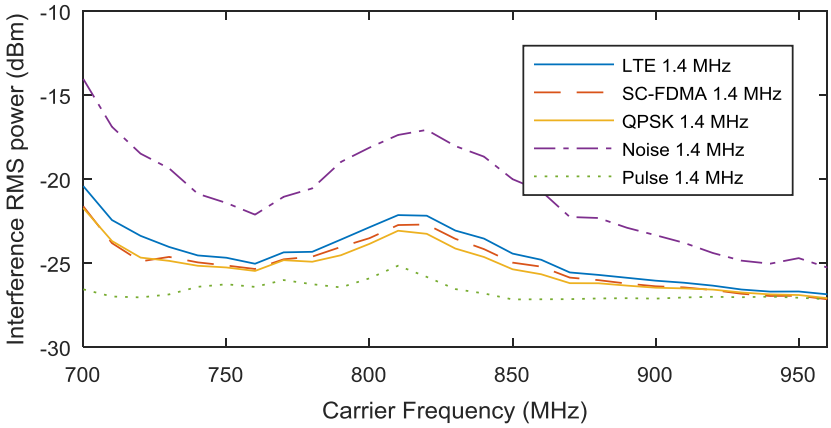

Figure 5.11: RMS power of interference signals, 1.4 MHz BW

The observations made with a carrier frequency of 700 MHz were valid for all other carrier frequencies: the filtered noise induced the highest RMS power; pulse modulated waveforms induced the lowest RMS power; LTE, SC-FDMA and QPSK induced a similar RMS power.

The RMS power values of the interference signals induced by waveforms with a channel bandwidth of 20 MHz are plotted in Fig. 5.12. The limits of the y axis were modified to improve the visibility of the traces.

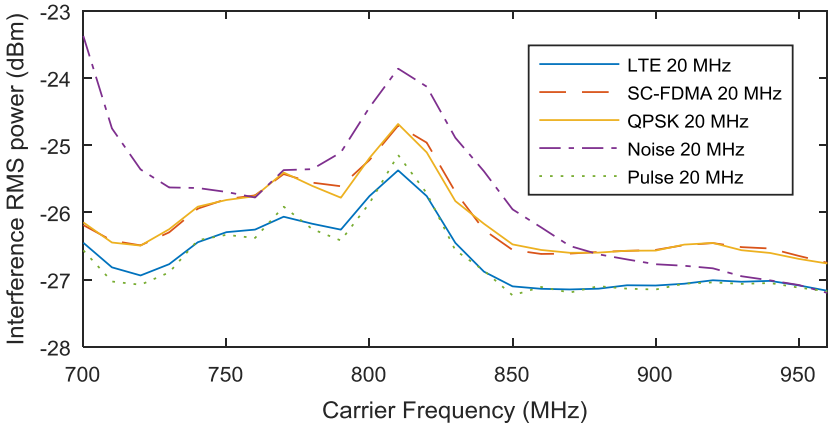

Figure 5.12: RMS power of interference signals, 20 MHz BW

The interference induced by the filtered noise had higher RMS power than that of other waveforms, except for carrier frequencies from 880 to 960 MHz, where the interference caused by SC-FDMA and QPSK had a higher RMS power than that of filtered noise. The interference induced by the filtered noise had a higher RMS power than that of LTE, except for carrier frequencies from 940 to 960 MHz, where the RMS power values were similar for both waveforms. It can be deduced that the RMS power of the interference induced by waveforms with a high channel bandwidth was more susceptible to variations caused by the change of carrier frequencies. For all carrier frequencies, the RMS power of the interference induced by the pulse modulated waveform was similar to that of LTE with a 20 MHz bandwidth, and the interference caused by the SC-FDMA waveform had similar RMS power values to that of QPSK.

An analysis was also done for the peak power values of the interference signals with different carrier frequencies. The peak power values of the interference induced by waveforms with a channel bandwidth of 1.4 MHz and carrier frequencies from 700 MHz to 960 MHz are plotted in Fig. 5.13.

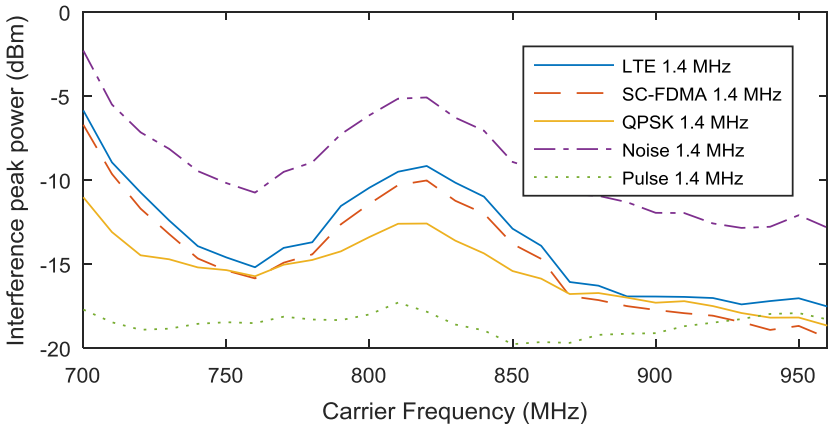

Figure 5.13: Peak power of interference signals, 1.4 MHz BW

For all carrier frequencies, the interference induced by the filtered noise with a channel bandwidth of 1.4 MHz had higher peak power than that of all other waveforms. The peak power values of the interference signals induced by all waveforms with a channel bandwidth of 20 MHz and carrier frequencies from 700 MHz to 960 MHz were plotted in Fig. 5.14.

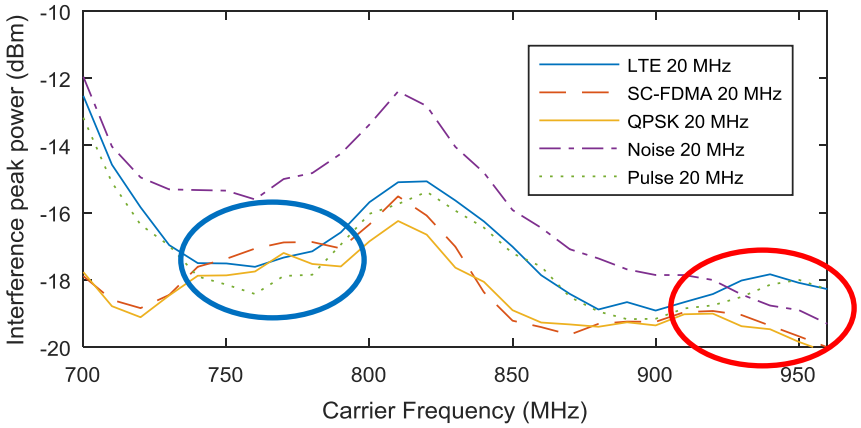

Figure 5.14: Peak power of interference signals, 20 MHz BW

The interference induced by the noise waveform had a higher peak power than that of all other waveforms, except for carrier frequencies from 920 to 960 MHz, as highlighted by the red circle. The interference produced by the LTE and pulse modulated waveforms had a higher peak power than that of SC-FDMA and QPSK, except for carrier frequencies from 740 to 790 MHz, as highlighted by the blue circle. The effect of the discontinuous transmission on the peak power was more significant for waveforms with higher channel bandwidths.

It was observed that, only when the bandwidth of a LTE waveform is much wider than the passband of the DUT, the interference induced by a pulse modulated waveform were representative of the interference caused by the LTE waveform. When the bandwidths of the test waveforms were smaller than 10 MHz, the SC-FDMA, QPSK, and filtered noise waveforms provided better representation of the interference produced by LTE than the pulse modulated waveform.

These observations did not validate the claim by the DO294C that the highest interference threat is linked to pulse modulation [4]. Waveforms with a high PAPR such as the filtered noise induced interference signals with significantly higher RMS and peak power values, especially for narrow channel bandwidths.

As the RMS and peak power of the interference induced by filtered noise with a channel bandwidth of 1.4 MHz were always higher than that of LTE, filtered noise with a small bandwidth could be adequate for radiated susceptibility testing: they over-estimate the amplitude variations of the LTE signals. If no radiated susceptibilities were found using a filtered noise waveform, the immunity to the LTE standard could be determined. Besides, noise waveforms could exceed the radiated susceptibility testing requirements for LTE: the filtered noise waveform could induce interference levels that were not present for the LTE waveforms.

5.4 Summary

Radiated susceptibility testing was used to compare the interference signals induced from the test waveforms that were previously designed. The PM1000II was chosen as a victim system, and its frequency response was evaluated.

It was found that discontinuous transmissions such as the blanking periods in LTE and in the pulse modulated waveforms have a significant effect on the peak power of the interference signals. In this case, continuous waveforms such as SC-FDMA with a similar PAPR to that of LTE, could not emulate the effects of discontinuous waveforms during radiated susceptibility testing. When bandwidth is increased, the effect of the discontinuous transmission on the peak power becomes more significant.

It was also found that the effect on the interference of an increase in the PAPR of the test waveforms was more significant than the effect of the discontinuous transmission. The RMS and peak power of the interference induced by the filtered noise waveforms were significantly higher than those of the interference from LTE. The use of filtered noise waveforms for radiated susceptibility testing is relevant.

When the bandwidth of a signal is much wider than the passband of the DUT, the interference induced by a pulse modulated waveform could be representative by a noise-like signal. However, when the bandwidth of the test waveforms was smaller than 10 MHz, the RMS and peak power values of the interference produced by the pulse modulated waveforms were significantly lower than that of LTE. Therefore, the validity of only using a pulse modulated waveform for radiated susceptibility testing can be rejected.

6 Conclusion

6.1 Summary

The EMC standards that were reviewed for the purpose of this thesis were found to rely heavily on a pulse modulated signal, with parameters that were representative of the GSM standard. However, previous research on radiated susceptibility testing showed that complex signals can induce susceptibilities that were not present for the pulse modulated signal. Different LTE signals were recorded and analyzed: the analysis showed that the peak power was normally distributed; that the OBW and the PAPR measurement of a LTE signal were not independent.

LTE, SC-FDMA, QPSK, uniform noise, and pulse modulated waveforms were designed using a parameter reduction process. The waveforms parameters were set such that their power spectrum matched the spectrum emission mask of the LTE standard. LTE and SC-FDMA waveforms had similar PAPR values; QPSK had a lower PAPR; filtered noise waveforms had a higher PAPR. Radiated susceptibility testing used the PM1000II intercom system as a victim to compare the interference signals induced from the different test waveforms, sweeping the carrier frequency from 700 to 960 MHz.

6.2 Conclusions

The discontinuous transmissions in the LTE and in the pulse modulated waveforms had a significant effect on the peak power of the interference signals. However, the effect the PAPR was more significant than the effect of the discontinuous transmission. In fact, the RMS and peak power of the interference induced by the filtered noise waveforms were significantly higher than those of all other waveforms. It is proposed that filtered noise waveforms can be used with confidence for radiated susceptibility testing.

The pulse modulated waveform were only representative of the LTE signal when the bandwidths of the LTE signals were much wider than the passband of the DUT. Otherwise, the interference levels produced by the pulse modulated waveforms were significantly lower than that of LTE. It is concluded that pulse modulated waveforms cannot be used alone for radiated susceptibility testing.

6.3 Contributions

The most important contribution of this thesis is a set of waveforms parameters that could be used to simulate the interference effects of the LTE communication standard. There are three secondary contributions of this thesis. The first is a method to analyze the parameters of a communication signals to extract the parameters for radiated susceptibility testing: for the first time, actual LTE signals were recorded at RMCC. The second is a parameters reduction process to simplify the testing of complex signals. The third is a method to validate the test signals for specific communication standards.

6.4 Future Work

Upon the completion of this thesis, the subject related to antennas for EMC immunity testing was found to require future work. In this thesis, a microstrip patch antenna was used to emulate the radiation pattern and gain of the planar inverted F antennas found in mobile devices. However, most patch antennas suffer from a relatively small bandwidth. It must be determined if microstrip patch antennas can used for EMC immunity testing. If not, antennas that can emulate the electromagnetic fields produced by a mobile device must be chosen.

Bibliography

[1] C. R. Paul, *Introduction to Electromagnetic Compatibility,* 2006, John Wiley and Sons, Inc.

[2] ETSI TS 145.005 "Digital cellular telecommunications system (Phase 2+) (GSM); GSM/EDGE Radio transmission and reception (3GPP TS 4.005 version 13.3.0 Release 13)", ETSI, Valbonne, France, Jan 2017.

[3] ETSI TS 136.101 "LTE; Evolved Universal Terrestrial Radio Access (-E-UTRA); User Equipment (UE) radio transmission and reception (3GPP TS 36.101 version 13.6.1 Release 13)", ETSI, Valbonne, France, Mar 2017.

[4] Radio Technical Commission for Aeronautics Special Committee SC-202, Document DO294C, "Guidance on allowing transmitting portable electronic devices on aircraft", RTCA Inc., Washington, DC, 2008.

[5] Radio Technical Commission for Aeronautics Special Committee SC-234, Document DO-307A, "Aircraft Design and Certification for Portable Electronic Device (PED) Tolerance", RTCA Inc., Washington, DC, Dec 2016.

[6] N. L. Armstrong and Y. M. M. Antar, "Investigation of the Electromagnetic Interference Threat Posed by a Wireless Network Inside a Passenger Aircraft" in *IEEE Transactions on Electromagnetic Compatibility*, vol. 50, no. 2, pp. 277-284, May 2008

[7] IEC 61000-4-3, "Electromagnetic compatibility (EMC) - Part 4-3: testing and measurement techniques - radiated, radio-frequency, electromagnetic field immunity test", International Electrotechnical Commission (IEC), 2010.

[8] MIL-STD-461G, "Requirements for the Control of Electromagnetic Interference Characteristics of Subsystems and Equipment", 2015.

[9] D. R. Kempf, "A comparison of the isotropic broadband susceptibility test method and an RS103 test on an ARC-182 radio," *Proceedings of IEEE Symposium on Electromagnetic Compatibility*, Chicago, IL, 1994, pp. 54-57.

[10] J.J. Ely, T.X. Nguyen and S.A. Scearce, "The Influence of Modulated Signal Risetime in Flight Electronics Radiated Immunity Testing with a Mode-Stirred Chamber", NASA Langley Research Center, Hampton, VA, Jan 2000.

[11] K. Nagase, S. Ishihara, J. Higashiayama, T. Onishi, and Y. Tarusawa, “Electromagnetic interference with medical devices from mobile phones using high-speed radio access technologies”, IEICE Communication Express, vol 1, no. 6, pp. 222-227, 2012.

[12] S. Ishihara, J. Higashiyama, T. Onishi, Y. Tarusawa and K. Nagase, "Electromagnetic interference with medical devices from third generation mobile phone including LTE," *2014 International Symposium on Electromagnetic Compatibility, Tokyo*, Tokyo, 2014, pp. 214-217.

[13] J.G. Proakis and M. Salehi, *Digital Communications, 5th Edition,* 2008, McGraw-Hill.

[14] 200-123-0003, “PM1000II Operator’s and Installation Manual”, PS Engineering Inc., Lenoir City, TN, Feb. 2012.

[15] 5991-0279EN, “M9381A PXIe Vector Signal Generator Data Sheet”, Keysight Technologies, Santa Rosa, CA, July 2015.

[16] HG908P-XX, “HyperLink Wireless 900 MHz 8 dBi Flat Patch Antenna Data Sheet”, L-Com Inc., North Andover, MA, July 2011.

[17] 3GW-20156-24, “Mixed Signal Oscilloscopes MSO4000B Series, DPO 4000B Series Data Sheet”, Tektronix Inc., Beaverton, OR, Jan 2016.